Fluid Inclusions and Microstructure of Flexural-Slip Bedding-Concordant Veins within the Ovens Anticline, Lunenburg, Nova Scotia

Darcy Edwin Lindsey Baker

Submitted in Partial Fulfillment of the Requirements
for the Degree of Bachelor of Science
Department of Earth Sciences
Dalhousie University, Halifax, Nova Scotia
March 1996

Distribution License

DalSpace requires agreement to this non-exclusive distribution license before your item can appear on DalSpace.

NON-EXCLUSIVE DISTRIBUTION LICENSE

You (the author(s) or copyright owner) grant to Dalhousie University the non-exclusive right to reproduce and distribute your submission worldwide in any medium.

You agree that Dalhousie University may, without changing the content, reformat the submission for the purpose of preservation.

You also agree that Dalhousie University may keep more than one copy of this submission for purposes of security, back-up and preservation.

You agree that the submission is your original work, and that you have the right to grant the rights contained in this license. You also agree that your submission does not, to the best of your knowledge, infringe upon anyone's copyright.

If the submission contains material for which you do not hold copyright, you agree that you have obtained the unrestricted permission of the copyright owner to grant Dalhousie University the rights required by this license, and that such third-party owned material is clearly identified and acknowledged within the text or content of the submission.

If the submission is based upon work that has been sponsored or supported by an agency or organization other than Dalhousie University, you assert that you have fulfilled any right of review or other obligations required by such contract or agreement.

Dalhousie University will clearly identify your name(s) as the author(s) or owner(s) of the submission, and will not make any alteration to the content of the files that you have submitted.

If you have questions regarding this license please contact the repository manager at dalspace@dal.ca.

Grant the distribution license by signing and dating below.

_____ _____

Name of signatory Date

Dalhousie University

Department of Earth Sciences
Halifax, Nova Scotia
Canada B3H 3J5
(902) 494-2358
FAX (902) 494-6889

DATE April 9, 1996

AUTHOR Darcy E. L. Baker

TITLE Fluid Inclusions and Microstructure of Flexural-Slip Bedding-Concordant Veins within the Ovens Anticline, Lunenburg, Nova Scotia

Degree BSc Convocation Dec. Year 1996

Permission is herewith granted to Dalhousie University to circulate and to have copied for non-commercial purposes, at its discretion, the above title upon the request of individuals or institutions.

Abstract

Fluid inclusions and microstructure of flexural-slip bedding-concordant quartz veins (FSBCVs) from the Ovens Anticl ine of the Meguma Group, were assessed and provide data on conditions and mechanisms of flexural-slip folding. These veins formed along flexural-slip movement horizons and are interpreted to have formed at the same time as flexural-slip folding.

Geobarometric results from planar fluid inclusion assemblages indicate that fluid pressure fluctuated and supralithostatic fluid pressures were present. Pressure results, when combined with an independent temperature of trapping (Tt), range from 0.5 to 5.0 kbars. The fluid was a mixed H_2O-NaCl-CO_2-CH_4 type.

FSBCVs contain abundant wall rock inclusion layers (WRILs) that originally were continuous but now are separated by layers of quartz. They host preferentially oriented fluid inclusion planes (FIP), and are composed of elongate quartz crystals which have a preferred crystallographic orientation with respect to elongation direction and possibly with respect to the fold. FIP orientation appears to be crystallographically influenced. These data suggest that the FIPs measured may not be healed microfractures and their orientation is therefore are not influenced by fold-related stress conditions.

Key Words: flexural-slip, fluid inclusion, supralithostatic pressure, laminated vein, Meguma Group

TABLE OF CONTENTS

TABLE OF FIGURES

ACKNOWLEDGEMENTS

I wish to thank Dr. Nick Culshaw, Rick Horne and Dr. Dan Kontak for expertise, thoughtfulness, and most of all patience. I have learned much from you. I also thank Dr. Martin Gibling for very helpful revisions and an informative and useful thesis class. To my parents: thanks for everything.

CHAPTER 1: INTRODUCTION

1.1 Background

The role of fluid pressure in faulting and folding of rocks in the upper levels of the crust has been acknowledged since Hubbert and Rubey (1959) argued that high fluid pressure can allow movement on faults that theoretically could not move if they were dry. In many cases, the horizontal stress required to cause movement on such a fault was calculated to be greater than the brittle strength of the rock. Such stress would fracture the rock rather than move it on a fault plane. Fluid pressure, however, counteracts vertical stress caused by gravity, thus reducing the effective body weight of the hanging wall and, in so doing, reduces the compressive stress required to move the fault (Hubbert and Rubey 1959).

Similar arguments were made by Price and Cosgrove (1990) for initialization of buckling in sedimentary sequences by flexural-slip. Flexural-slip folding occurs when a sedimentary sequence shortens by slip along bedding-concordant surfaces (analogous to a series of reverse faults on fold limbs). According to theoretical arguments by Price and Cosgrove (1990), high fluid pressure is required to counteract body weight of a sedimentary sequence during the formation of large wavelength (greater than a few tens of metres) flexural-slip folds. As in fault movement, without the effect of fluid pressure the shear stress on a potential flexural-slip plane would exceed the brittle strength of the rock for many observed folds (Price and Cosgrove 1990).

The presence of fluids during folding of sedimentary sequences can be recorded by

veins (Cox *et al.* 1991; Cosgrove 1993). Vein formation is generally considered to result from hydraulic fracturing which occurs when the least principal stress acting on the sedimentary sequence is exceeded by fluid pressure. These conditions cause fracturing and the space created is subsequently occupied by fluid which precipitates vein material. Cosgrove (1993) described this process as cyclical during fluid pressure influenced flexural-slip movement: (a) hydraulic fracturing occurs locally followed by, (b) migration of fluid away from the site of fracturing along the movement horizon causing slip to cease at this location as the plane 'locks up', (c) further increase of fluid pressure will cause this to repeat. Composite vein structures support this 'stick-slip' model (Cosgrove 1993).

Cox *et al.* (1991) reported that the formation of auriferous veins in the metasedimentary fold belts of Central Victoria State, Australia, was controlled by fold and thrust geometry and occurred in fractures formed by supralithostatic pressures (i.e. fluid pressure > lithostatic pressure, as in hydraulic fracturing). In addition to geometrical evidence of fluid fluctuation, vein textures and microstructure can record repeating episodes of vein formation.

This Australian fold belt has been compared to the Meguma Group of Nova Scotia in age, structure and lithology. Both of these geological units have long histories of gold production through mining of auriferous lode (vein) deposits. Flexural-slip was not recognized as an important folding mechanism in the Meguma Group until Horne (1993) documented clear field evidence for late-stage folding by flexural-slip at two Meguma Group locations: the Ovens Anticline near Lunenburg and the railway tracks section in the south end of Halifax. Since the Ovens Anticline is a former gold district, evidence of

flexural-slip implies that a re-evaluation of Meguma Group deposits may find that flexural-slip is an important mechanism of folding and an important factor influencing the formation of auriferous veins. Research conducted on the Australian deposits discussed above has concluded that generally these deposits are structurally controlled and related to flexural-slip (Cox *et al.* 1991; Cox 1995; Jessel *et al.* 1994). Despite the observations made at the Ovens, little is known about the fluid pressure conditions of this folding event.

1.2 Objectives

The objectives of this thesis are to examine the fluid pressure conditions of late-stage flexural-slip folding of the Ovens Anticline and to investigate the nature and microstructure of veins that formed during flexural-slip. Oriented samples of flexural-slip veins (formed along flexural-slip movement horizons) were collected and their microstructure determined, described and compared with the expected flexural-slip model. A thermometric investigation of fluid inclusions in these samples constrains vein formation (and therefore flexural-slip) pressure conditions.

1.3 Regional Geological Setting

Nova Scotia is divided tectonically by the Cobequid-Chedabucto fault system: north of this system lies the Avalon Terrane and to the south lies the accreted Meguma Terrane. From oldest to youngest, the Meguma Terrane consists of : (a) the metasedimentary, Cambro-Ordovician Meguma Group (Schenk 1991), (b) conformably overlying Silurian-Devonian metasedimentary and metavolcanic rocks, (c) Devonian granitoids, and (d)

unconformable late-Paleozoic to Mesozoic terrigenous and marine sedimentary and volcanic rocks (Fig. 1.1). The Meguma Group and overlying Silurian-Devonian rocks were metamorphosed and deformed into widespread, NE-SW-trending, kilometre-scale folds during the mid-Devonian Acadian Orogeny (Keppie and Dallmeyer 1987; Muecke *et al.* 1988). Metamorphic grades range from greenschist to amphibolite facies and rocks are locally overprinted by contact metamorphism from Devonian granitoid intrusions (Clarke *et al.*1988).

The Meguma Group consists of the lower meta-sandstone-dominated Goldenville Formation and the upper slate-dominated Halifax Formation. This group became of economic interest with the discovery of gold about 1860 (Faribault 1899). Since that time, 63 gold districts, mostly within the Goldenville Formation, have produced 1.2 million ounces of gold from quartz vein deposits. Localization of these veins is usually controlled by structure, because deposits are hosted by antiforms, shear zones or fault zones.

1.4 Previous Work on Meguma Group Veins

Henderson *et al.* (1986) provide a comprehensive folding history of the Meguma Group. The stages of this model are: (a) supralithostatic fluid pressure developed within flat-lying sediments resulting in hydraulic fracturing and formation of early bedding-concordant veins, (b) layer-parallel shortening of the sedimentary sequence resulted in cleavage development normal to bedding and symmetric buckling of veins formed in stage (a) as well as more competent lithologic beds, and (c) fold development and passive cleavage rotation by flexural shear. Horne and Culshaw (1994) have shown that folding of

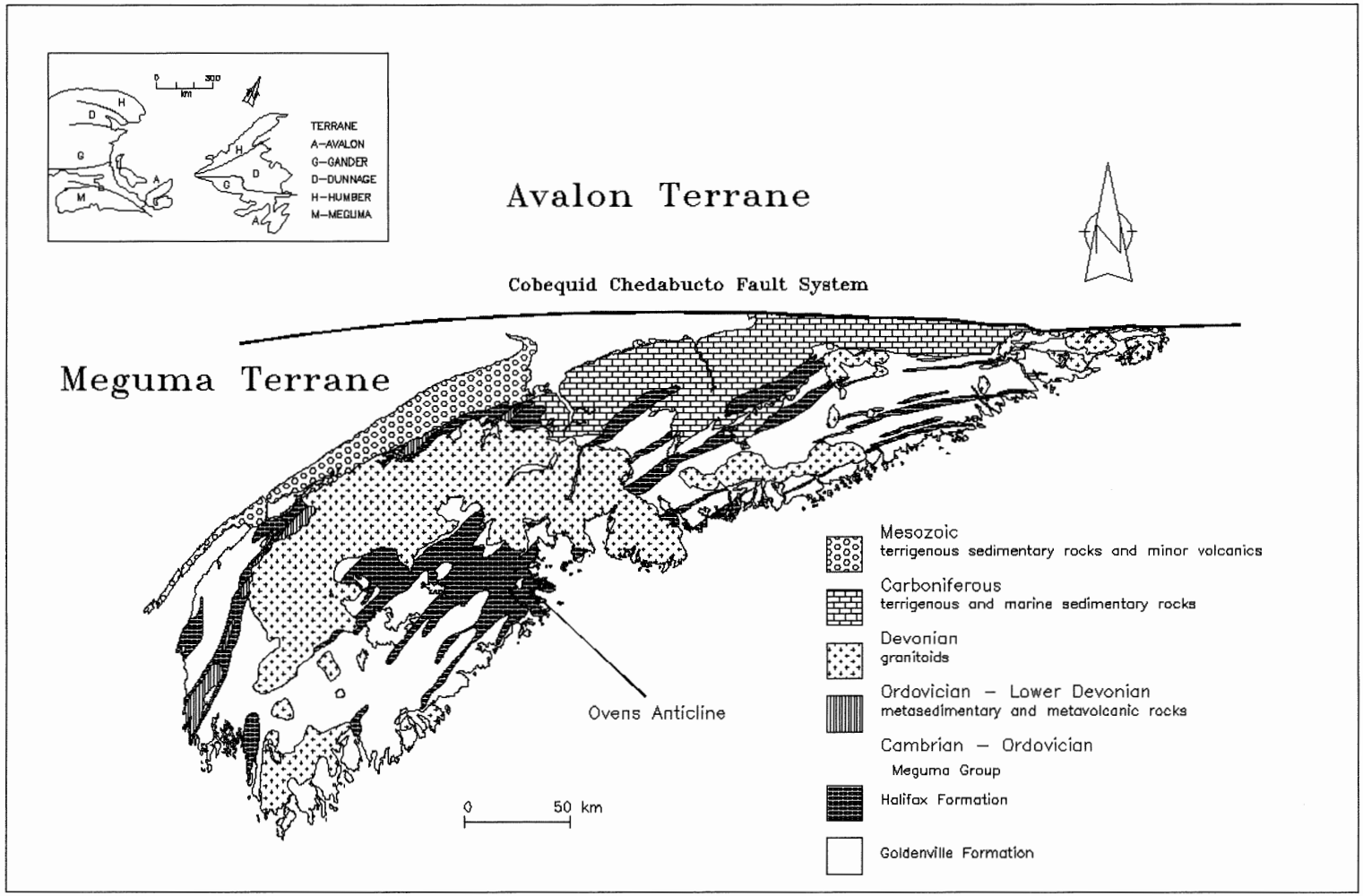

Figure 1.1 Geological map of the Meguma Terrane showing the location of the Ovens Anticline (courtesy Nova Scotia Department of Natural Resources).

the Ovens Anticline was partially accomplished by flexural-slip and that most vein formation occurred late with only minor vein formation early in the fold history (as described by model of Henderson *et al.* (1986)).

Despite considerable investigation into Meguma Group gold occurrences, little consensus exists on the formation mechanism(s) responsible for vein emplacement. Previous work has produced the following explanations for Meguma Group vein genesis: (1) veins formed from hydrothermal fluids active during marine sedimentation (Haynes 1986), (2) veins formed by hydraulic fracturing before folding (Graves and Zentilli 1982; Henderson and Henderson 1986), (3) veins formed during folding (flexural-slip, saddle reef model) (Faribault 1899; Keppie 1976; Mawer, 1986, 1987; Horne and Culshaw 1994), (4) veins formed after folding related to regional shear zones (Kontak *et al.* 1990), and (5) vein formation related to emplacement of Devonian granitoids (Newhouse 1936; Douglas 1948).

CHAPTER 2: THE OVENS ANTICLINE

2.1 Description Of The Ovens Anticline

The Ovens Anticline is exposed at two coastal locations on both sides of a peninsula (Fig. 2.1a) and defines a classic chevron-style fold (Fig. 2.2). Ramsay (1974) outlined the following general features of chevron folds: (1) chevron folds have straight limbs, (2) they occur in sedimentary sequences with two alternating, regularly bedded units of differing competency, (3) stratigraphic thickness of competent units remains constant (i.e. a parallel fold), (4) stratigraphic thickness of less competent units may vary in the hinge zone, and (5) less competent units commonly show ductile flow.

The Ovens Anticline has formed in the Cunard Member of the Halifax Formation (O'Brien 1988). Local stratigraphy consists of approximately 70% slate and 30% meta-sandstone. The fold limbs are straight and the interlimb angle is 35° - 40° (Fig. 2.2). The axial plane trends northeast and dips steeply northwest; cleavage within the anticline is axial planar (Fig. 2.1b). An exception occurs locally on the south limb where outcrop-scale thrusts resulted in a large bedding-cleavage angle on a steeply dipping limb. The Ovens Anticline hosts abundant quartz veins that differ considerably in size and morphology. Veins are generally much less common away from the hinge zone.

2.2 Quartz Veins

Four different types of quartz veins within the Ovens Anticline have been described by Horne and Culshaw (1994) and are schematically shown in Figure 2.3: early bedding-

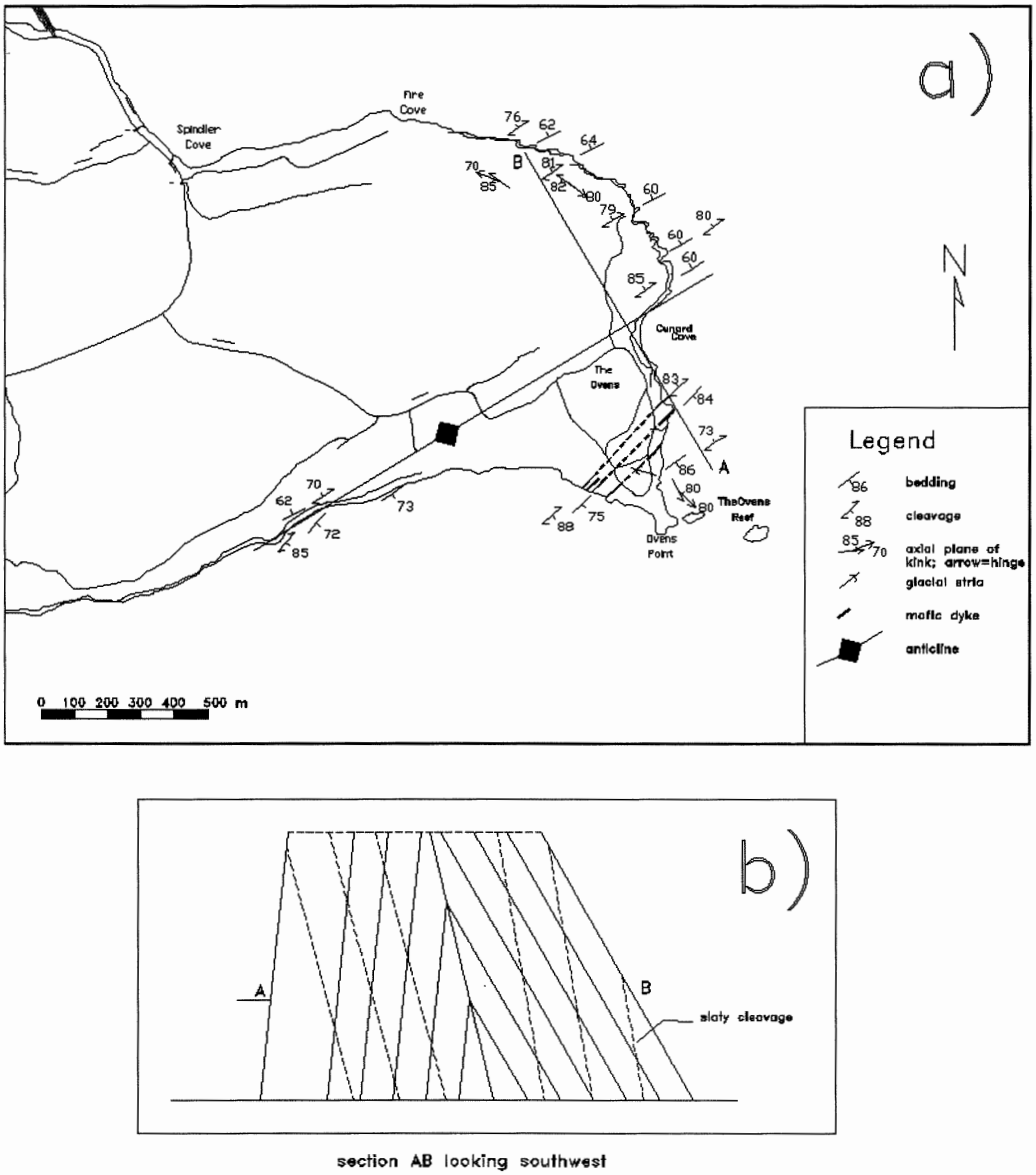

Figure 2.1 The Ovens Anticline (a) in map view . Locations of samples studied in detail are included. Cross-section A-B of the Ovens Anticline (b) illustrating general bedding-cleavage relationships across the fold. Cleavage is axial-planar, dipping steeply NW.

Figure 2.2 Photograph of the Ovens Anticline hinge zone looking NE. Chevron geometry is shown by white lines (Photo courtesy of R. Horne, Nova Scotia Department of Natural Resources).

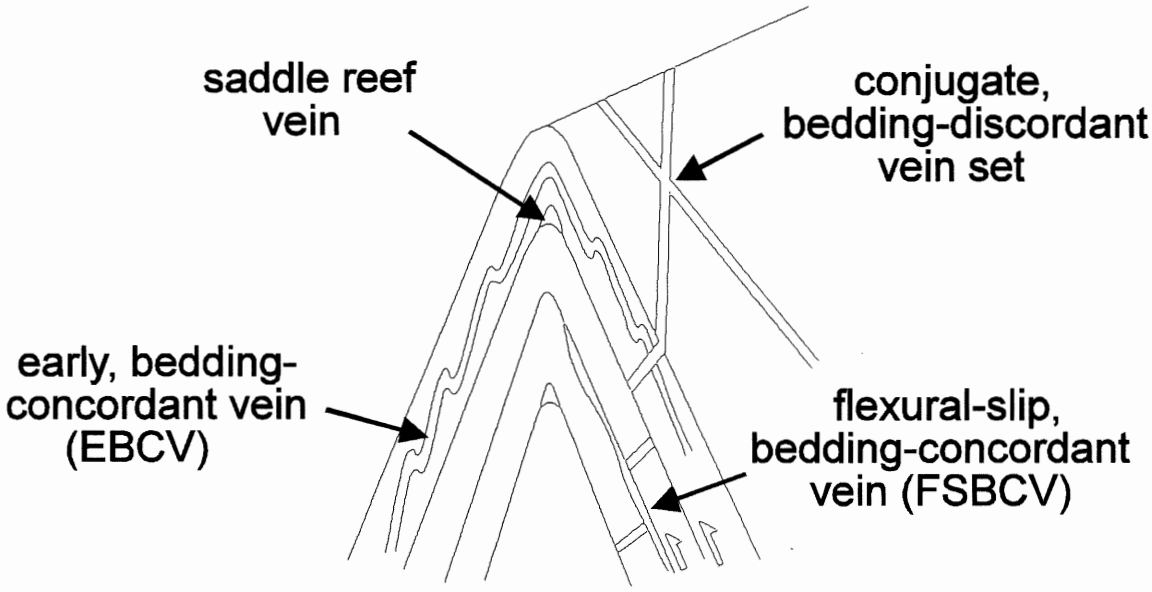

Figure 2.3 Schematic diagram of the four quartz vein types recognized within the Ovens Anticline. See text for description of relationships (after Horne and Culshaw 1994).

concordant (EBCV), flexural-slip bedding-concordant (FSBCV), saddle reef, and a conjugate set of bedding-discordant veins exist. FSBCVs are concordant with flexural-slip movement horizons and are interpreted to have formed during flexural-slip folding (Horne and Culshaw 1994). FSBCVs and bedding-discordant veins comprise the majority of veins within this hinge zone. Based on cross-cutting relationships, bedding-discordant veins formed coevally with FSBCVs and therefore coevally with flexural-slip folding. Study of these veins where they intersect show that some bedding-discordant veins formed before or during flexural-slip because the veins are offset at a FSBCV (i.e. a flexural-slip movement horizon) (see cross section view of bedding-discordant veins of Figs. 2.3 and 2.4). A second bedding-discordant vein, however, may cut across this movement horizon without showing offset therefore indicating it formed after flexural-slip occurred on the movement horizon.

Saddle reef veins are locally exposed at the hinge of the Ovens Anticline. They are approximately 20-25 cm thick (at the hinge) and rapidly taper down-dip to a thickness of a few centimetres. Saddle reef veins occupy fold-related hinge dilatant zones and, therefore, are late-stage veins. In accordance with the general saddle-reef model of vein formation, FSBCVs are likely related to the saddle reef veins because the saddle may be a FSBCV that thickens at the hinge simply because there was room for it to do so. This relation is described by Cox *et al.* (1991) for the Lachlan Fold Belt of Australia where underground mining has shown that saddle reefs taper down-dip to 'leg reefs' which are similar to FSBCVs.

Compared with FSBCVs and bedding-discordant veins, very few EBCVs are

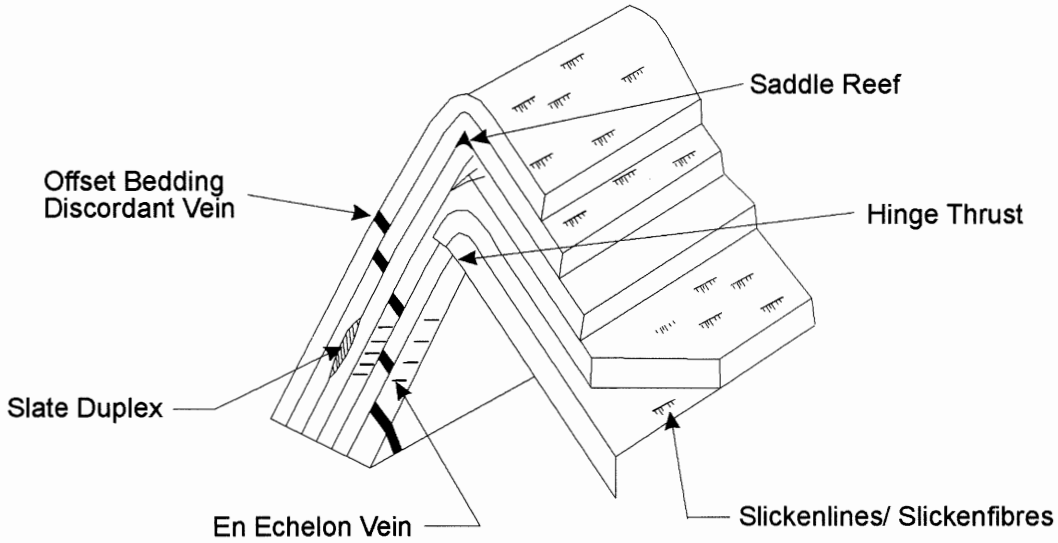

Figure 2.4 Schematic diagram of a flexural-slip fold showing structures described by Tanner (1989).

present. Asymmetric parasitic folding of these veins defines them as pre-shortening and therefore pre-folding based on the model of Henderson *et al.* (1986) described above. These veins are generally small with thicknesses up to, but generally much less than, 1 cm.

The relative abundance of FSBCVs (including saddle reefs) and bedding-discordant veins close to the hinge compared with the lack of these veins down the limbs, indicates that the fold hinge acted as a trap for fluids responsible for vein deposition (Horne and Culshaw, 1994). The abundance of EBCVs, because they formed before folding, is not expected to increase in the hinge but should remain constant throughout the fold.

2.3 Structure

As mentioned in Chapter 1, flexural-slip is movement on surfaces that are concordant with stratigraphic horizons during folding of regularly bedded rock sequences (Tanner 1989). During flexural-slip folding of an antiform, beds above a movement horizon move toward the fold hinge (up-dip), relative to those beneath the movement horizon (Fig. 2.4). Bedding-concordant structures associated with the formation of a flexural-slip fold include slickensided surfaces, slickenfibres, slate duplexes and quartz veins. Accommodation structures (Ramsay 1974; Price and Cosgrove 1990) may locally occur in fold hinges and extensional en echelon veins may form (Fig. 2.4). Study of large flexural-slip folds, particularly quantifying offset on flexural-slip movement horizons, is inherently limited by exposure.

The presence of bedding-discordant quartz veins, which provide offset markers of bedding-concordant slip, and the extensive outcrop of this coastal location, make the

Ovens Anticline an excellent site for study of flexural-slip. Slate duplexes, slickenlines and slickenfibres as well as offset bedding-discordant veins, provide evidence of flexural-slip folding. Figure 2.5 shows a slate bed deformed into a duplex structure consisting of flats and ramps that indicate a shear direction consistent with flexural-slip movement. Slickenlines and more rarely slickenfibres (Fig. 2.6) developed to various degrees along bedding-concordant movement horizons and indicate slip direction. The hinge exposure locally shows thrusting (accommodation structure). Bedding-discordant veins form a systematically oriented conjugate set with west-dipping and steeply dipping groups. Where discordant veins from both of these groups can be observed to have been offset at a movement horizon, a true offset can be accurately determined as the ambiguities of observing only one offset marker (i.e. an apparent offset) are diminished.

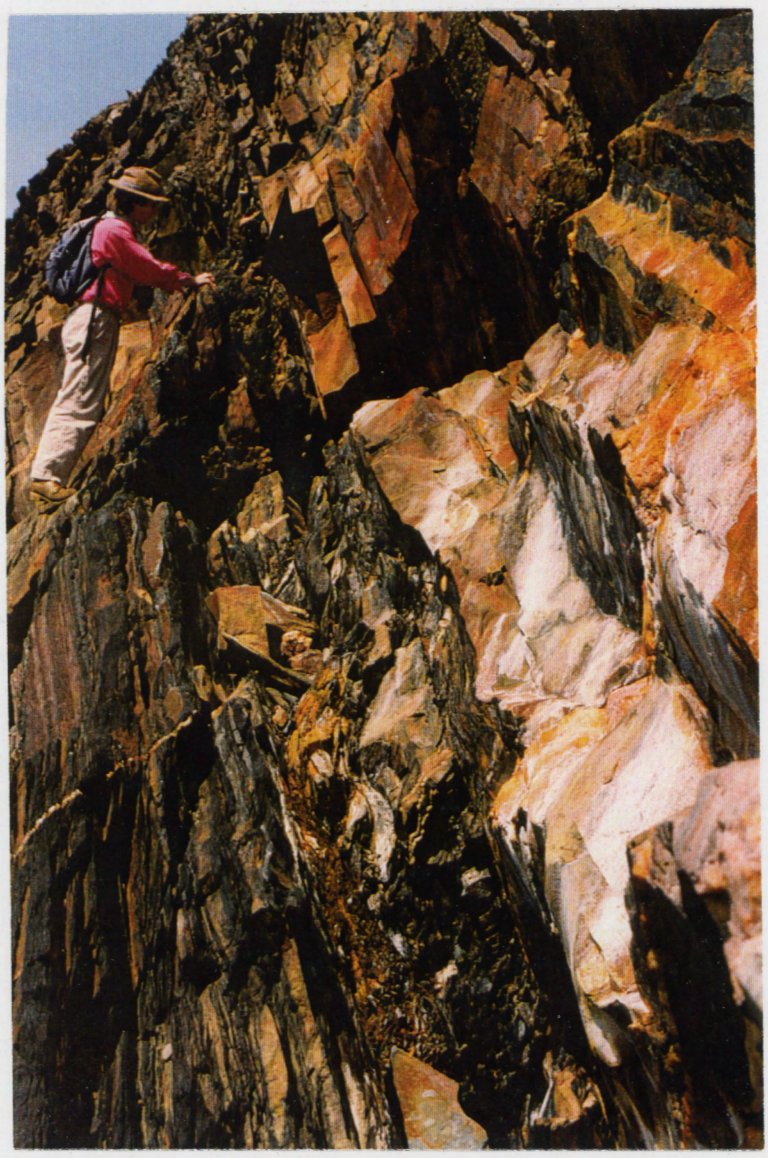

Figure 2.5 Photograph showing a well-developed slate duplex (immediately above man's hand) on the NW limb of the Ovens Anticline. Ramp and flat geometry of this structure shows that rock above (right-hand side of photo) this structure moved up relative to rock below the structure. This is consistent with flexural-slip.

Figure 2.6 Slickenfibres on a bedding-concordant flexural-slip movement horizon showing the direction of flexural-slip movement (Photo courtesy of R. Horne, Nova Scotia Department of Natural Resources).

CHAPTER 3: SAMPLES AND METHODS

3.1 Sample Selection

Thirty-three quartz veins of various types were sampled from coastal exposure of the Ovens Anticline in August, 1995. Vein orientation, sample location and sample orientation were recorded to allow vein structure to be studied with respect to regional folding. Polished thin sections were produced from 14 of these samples, generally two sections from each sample: one parallel to vein dip, and the other parallel to the vein strike.

Although all vein types were sampled, only FSBCVs were studied in detail. Fluid inclusions in six FSBCVs were assessed in order to determine type (liquid, liquid-vapour, liquid-vapour-solid, or vapour), shape, genetic history (primary, secondary, pseudosecondary), and size. Three samples (O-60, O-82, and O-83), were selected for thermometric and detailed petrographic analysis. Doubly-polished, 150 micron-thick fluid-inclusion sections of these samples were produced, in two orientations as described above.

3.2 Methods

This thesis uses thermometric determinations of planar arrays of fluid inclusions and detailed qualitative and quantitative petrographic analysis to model the mechanism and conditions of FSBCV formation. The study is divided into three steps: (a) quantitative and qualitative assessment of microstructures by standard petrographic observation, (b) classification of fluid inclusions and measurement of the planar orientation of isolated fluid

inclusion assemblages (referred to as fluid inclusion planes, or FIP, if a planar orientation is exhibited), and (c) determination of the pressure-temperature-composition (P-T-X) conditions of individual fluid inclusions via thermometric measurements. The last step is of limited use without the constraints imposed by careful petrographic observations in (a) which provide critical timing relationships.

3.2.1 Assessment of Microstructures

Standard, 30 micron-thick polished thin sections were studied to assess microstructure of FSBCVs. A transmitted-light petrographic microscope was used with 1, 2, 4, 10, 20, 40, and 100x objectives lenses and 10x ocular lenses containing a graduated E-W cross-hair.

Quantitative analyses of included sub-parallel wall-rock layers (see below for further discussion) and crystallographic orientation of quartz crystals; and qualitative assessment of deformation textures were conducted. Thin section traverses were conducted perpendicular to included wall-rock layers with the use of a mechanical stage. Thicknesses of wall-rock inclusion layers and the quartz layers that separate them were measured using the graduated cross-hair. Traces of crystallographic c-axes were determined by determining the slow extinction direction. This was accomplished using standard petrographic techniques (i.e. use of a tint plate to observe increases or decreases in birefringence colours). The c-axis traces and crystal boundaries were recorded on photomicrographs of the thin sections. A Universal stage was also used to measure the exact c-axis orientation of two quartz crystals. Qualitative assessment was conducted

using photographs, sketches and notes.

3.2.2 Fluid Inclusion Assessment

Fluid inclusions were assessed and pre-selected for thermometric study. Groups of large inclusions (so phase changes could be resolved during heating and cooling experiments) that clearly have a planar orientation (i.e. fluid inclusion planes: FIPs) were chosen. Planar orientation of these inclusion populations is recognized by adjusting the focal depth of the microscope through the thickness of the thin section. As this is done, a FIP appears as a linear feature which sweeps back and forth parallel to the dip of the plane. Inclusions that were not clearly a member of a planar inclusion population, or were found in areas of high inclusion density (e.g. where numerous FIPs intersect) were avoided. Their locations were recorded using detailed maps and whole-thin-section photomicrographs so they could be relocated on the heating/cooling stage. Re-orientation of the sample chips once removed from the slide was accomplished by marking each edge of the sample with a different colour and recording this as well as chip shapes in detailed sketches. Any selected inclusion could then be found at a later time.

FIP orientations were measured using a technique similar to that of Selverstone *et al.* (1995). The modified procedure used for measuring inclusion plane orientations is as follows: (a) the stage was rotated so the plane was parallel to the north-south cross hair, dipping to the right and the azimuth was recorded from the graduated stage; (b) focus was achieved on the highest inclusions in this plane and values from the graduated fine focus knob and from the point on the east-west graduated cross-hair where these inclusions

were visible were recorded; (c) focus was achieved on the lowest resolvable inclusions in the plane and values from the fine focus knob and the cross-hair were again recorded. The differences of the focus knob values provides a thickness, T, of measured plane perpendicular to the section, and the difference of cross-hair values provides a width, W, of that same amount of plane parallel to the thin section. The dip of fluid inclusion plane was given by:

$$\tan^{-1}(T/W) = \text{delta} \quad (3.1)$$

This was combined with the azimuth (strike) from (a) for a complete orientation. Traverses across thin sections were conducted before removal from the glass slide to measure FIP orientations.

Because this method uses a flat-stage, it is acknowledged that measurement of FIPs that are at a low angle to the thin section is difficult to impossible. In general, only FIPs that dip >15° to the thin section surface can be measured because at angles lower than this it is not possible to accurately view the linear feature (i.e. the individual inclusions that are in focus) sweep back and forth with focus adjustment. To correct for this, measurements were taken from two thin sections cut at right angles from the same sample as described above. These data were then combined and plotted together.

Raw FIP measurements were taken in reference to the top of the thin section. These data were rotated into 'real space' so FIPs could be assessed with respect to the fold. Rotation was accomplished using the computer software *Spheristat* 2.0. Errors during sawing vein samples resulted in thin sections that were up to 8° oblique to vein dip or strike. Some samples were placed on thin sections so that vein margins were oblique

(up to 4°) to the edges of the glass plate. These factors were also corrected for by rotating data.

3.2.3 Fluid Inclusion Microthermometry

3.2.3.1 Background

Fluid inclusions form during the growth of crystals, but also during the healing of cracks or fractures formed by stress acting on a crystal (Roedder 1984). Figure 3.1 illustrates schematically the different genetic types of fluid inclusions. Fluid inclusions trapped during growth of the host crystal are termed primary and form by overgrowth of defects or irregularities on crystal surfaces, thereby trapping fluid that is present at the time of crystal formation (Roedder 1984). Inclusions also become trapped by healing of microfractures or by dissolution-precipitation mechanisms (Goldstein and Reynolds 1994); such inclusions are termed secondary. A third category of fluid inclusion, termed pseudosecondary, are trapped when fractures or cracks in a crystal heal while the crystal is still undergoing primary growth.

Fluid inclusions provide physical and chemical information in many ways. Fluid inclusion applications generally rely on the premise that the fluid contained in these voids represents the fluid responsible for precipitation of the host mineral and that the chemical phase changes that occurred during cooling, are reversible (Roedder 1984). By heating and/or cooling fluid inclusions, observing and recording the temperatures at which phase changes occur, and with knowledge of the nature of the fluid contained in the inclusion, the temperature of trapping (Tt) or the pressure of trapping (Pt) of inclusions can be

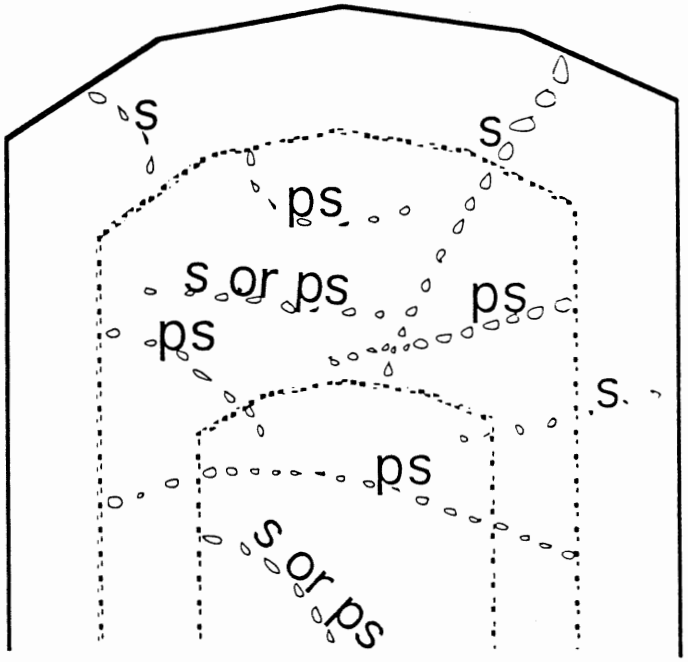

Figure 3.1 Schematic diagram of a crystal which hosts primary fluid inclusions (outlining crystal faces), secondary fluid inclusions (s), and pseudosecondary fluid inclusions (ps). Primary fluid inclusions are identified as those that outline crystal growth zones. Secondary fluid inclusions are confined to planes that transect the crystal. Pseudosecondary fluid inclusions are identified where many fluid inclusion planes end at a common boundary such as the face of a growing crystal at the time fractures were healed trapping the pseudosecondary inclusions (from Roedder 1984).

calculated. If fluid boiling during inclusion entrapment can be demonstrated both Tt and Pt can be determined. In absence of boiling, independent determination of the other variable is required. That is, fluid inclusion geothermometry requires an independent estimate of Pt and fluid inclusion geobarometry requires an independent estimate of Tt.

3.2.3.1.1 Assumptions

Roedder (1984, p. 267) outlines six assumptions which form the basis of fluid inclusion geobarometry:

1. No change in the size of fluid inclusions has taken place since formation. Calculations treat fluid inclusions as closed systems and as such a change in inclusion shape would change the volume, pressure and density of the inclusion causing errors. This is usually a minor factor when size has changed slightly.
2. No change in inclusion content has occurred. Occasionally fluid inclusions leak and material is either removed or added to the inclusion.
3. The Tt is known or can be estimated to a high degree of accuracy.
4. The origin of the inclusion is known.
5. The results are not only precise (reproducible), but accurate.

Each of the above assumptions, if unfounded, can greatly affect the accuracy of results.

3.2.3.1.2 Use of data

The temperatures at which phase changes occur within fluid inclusions provide information on the trapping pressure when combined with known phase behaviour. The

general procedure for application of these methods involves determination of the composition of the phase or phases present in the inclusion. Experimental data on the behaviour of these phases through P-T space allow plotting of an isochore (equal density) line in P-T space.

Increased salinity of an aqueous (H_2O + NaCl) inclusion will decrease the melting temperature (Tm) of ice formed when an inclusion is cooled. Tm H_2O is therefore an indicator of salinity when compared with known NaCl-solution freezing values. Figure 3.2 shows the effect of salinity on Tm of ice (Curve B). The presence of CO_2 (i.e. a carbonic inclusion) adds two complications to salinity determination (Roedder 1984). First, dissolved CO_2 in water will also depress Tm. However CO_2 is not highly soluble in water so this factor is not great. Second, formation of a CO_2 hydrate (clathrate) generally occurs upon cooling a carbonic inclusion. Since this involves the combination of water with CO_2, the liquid water remaining (i.e. not combined as CO_2 hydrate) will have an increased salinity. This would further reduce the freezing point and add error to calculation of salinity values. Due to this factor, if clathrate formation occurs in inclusions, the Tm of clathrate is used to calculate the salinity of the aqueous phase using known experimental data of this system.

Carbon dioxide concentration is derived from known solubilities of CO_2 in water. In NaCl solutions, the solubility of CO_2 changes from the normal H_2O-CO_2 system. Published data are available detailing the solubility of CO_2 in NaCl solutions for a range of temperature and weight percent NaCl. Generally, CO_2 solubility decreases with increasing NaCl content ("salting out" effect); (Ellis and Golding 1963). With increasing temperature

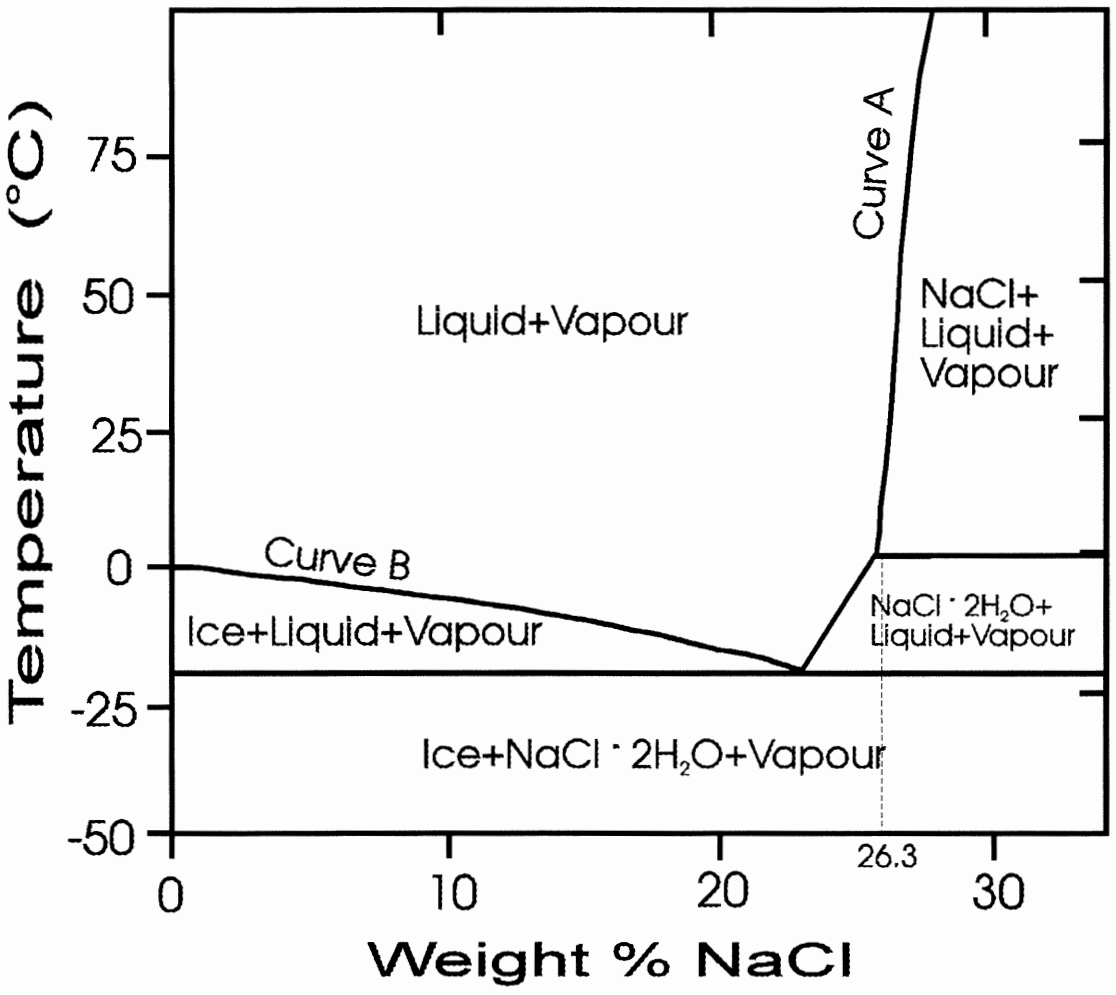

Figure 3.2 Experimental T-X plot for the low temperature, low salinity portion of the system H_2O-NaCl. Pressure is constant. Observed phase changes in aqueous fluid inclusions occurred at Curves A and B and provide salinity determination (from Goldstein and Reynolds 1994).

the salting-out effect falls to a minimum at about 150° C, but with higher temperatures it again increases because the critical temperature of the system is raised by the dissolved salt (Ellis and Golding 1963). The homogenization temperature (Th) of an inclusion is the temperature at which it forms one phase. The intersection of the Th of carbonic inclusions with the critical curve of Figure 3.3 provides the CO_2 content of the inclusion provided that the salinity of the aqueous portion of the inclusion is known. The Th of these inclusions, however, is seldom recorded because from Figure 3.3 it is noted that inclusions with minor amounts of CO_2 homogenize at high temperatures and pressures. The internal pressure of an inclusion at these conditions generally causes decrepitation of the inclusion before Th is reached. Experimental data must be available for the given NaCl concentration of the inclusion or the solubility must be interpolated from data of similar NaCl concentrations. Calculating the actual CO_2 content requires estimation of the volumes of CO_2 and H_2O. Such an approximation is affected by irregularity of the inclusion shape perpendicular to viewing direction.

Determination of Pt involves the use of known phase equilibria pressure-temperature diagrams for the system present in the inclusion. Figure 3.4 shows a P-T phase diagram for the H_2O-NaCl system with isochores (lines of constant density) plotted for different salinities. The point on the liquid-vapour curve at which Th plots corresponds to the isochore that originates at this point. This isochore represents the path through P-T space that a given inclusion will follow. Intersection of an independent Tt with this isochore provides the point in P-T space at which the inclusion was trapped and, therefore, Pt can be obtained from the pressure axis.

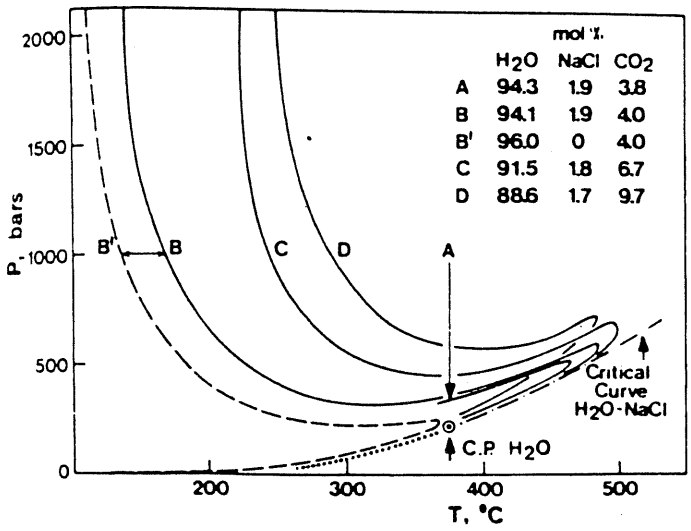

Figure 3.3 Equal composition phase boundary curves for the system H_2O-CO_2-NaCl. Notice the high temperatures which must be attained to homogenize inclusions containing significant CO_2. These inclusions frequently decrepitate before Th is reached due to high internal pressures that develop in CO_2 bvearing inclusions (from Gehrig *et al.* 1979).

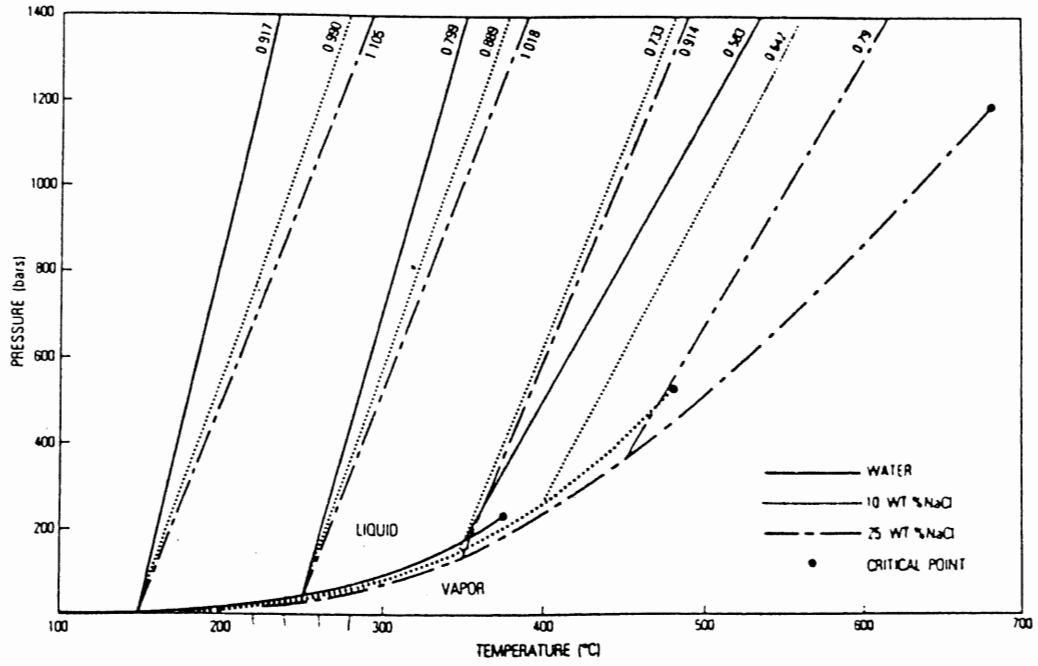

Figure 3.4 Pressure-temperature diagram for the system H_2O-NaCl. The curved line is the liquid-vapour curve separating these phases. The straight lines are isochores (lines of equal density). Such diagrams are used for plotting Th to find the inclusion density which is combined with an independent Tt to find the Pt (from Roedder, 1984).

3.2.3.2 Procedure for current study

Selected fluid inclusions were studied and thermometric measurements made using a United States Geological Survey (USGS) style fluid inclusion stage (Fig. 3.5) which is mounted on a petrographic microscope equipped with 5, 10, 32, and 40 x objective lenses and 12.5 x ocular lenses. The microscope is also attached via a video camera to a monitor and images can be reproduced with a black and white Sony video graphics printer. This stage allows chemical and physical phase changes, which occur within fluid inclusions during temperature change, to be observed and the temperature at which they occur to be recorded. The USGS stage provides continuous flow of heated or cooled gas around the sample chip; in the case of heating compressed room air is used, whereas for cooling N_2 gas is used. The small volume of material to be heated or cooled compared with the volume of hot/cold gas which is passed around it allows for very rapid temperature cycling (Roedder 1984). This is important for attaining precise and accurate measurement of the temperatures of phase changes.

The procedure used in this study involved the location of selected inclusions using standard petrographic techniques as described above. An image of each inclusion studied was obtained at room temperature with the video graphics printer. Freezing experiments were completed on all fluid inclusions for each sample chip prior to conducting heating experiments. Inclusions containing condensable gases (e.g. CO_2 or CH_4) develop high internal pressures upon heating, therefore care was taken to heat selected inclusions, within a single chip, incrementally to avoid decrepitating inclusions. For example, the first inclusion studied on a chip was not taken to its homogenization temperature if this

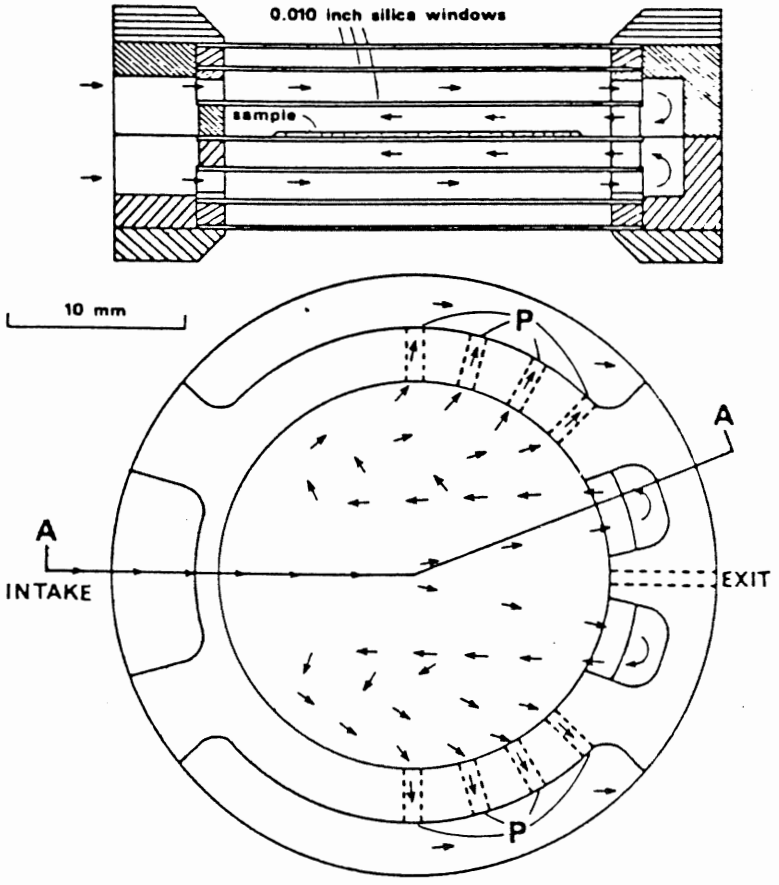

Figure 3.5 United States Geological Survey (USGS) type freezing stage used for thermometric fluid inclusion measurements. Arrows represent the flow paths of hot or cold air directed above and below the sample chip. P is portals for air escape; A-A is crossection (from Roedder 1984).

temperature was excessive, until inclusions that homogenized at lower temperatures were studied.

Table 3.1 summarizes the data collected for the three chemical systems encountered in this study. These data were entered into the computer software program, *Flincor*, which uses melting and/ or homogenization temperatures with pre-programmed, experimental density curves to output a table of pressure-temperature values. These were hand plotted in P-T space to provide an isochore, or line of constant density. Based on the chemistry of an inclusion its position in P-T space must lie on its isochore since an inclusion is a closed system and therefore has constant density.

SYSTEM	DATA RECORDED	PROVIDES
H_2O-NaCl	Tm H_2O	salinity/ density
	Th	minimum trapping temperature of inclusion
H_2O-NaCl (with solid NaCl)	Tdissolution NaCl	salinity/ density
	Th	minimum trapping temperature of inclusion
H_2O-CO_2-NaCl	Tm clath	salinity/ density of H_2O-NaCl portion of inclusion
	Th CO_2	density of CO_2 portion of inclusion
	Vol. fractions of CO_2/H_2O	bulk inclusion density
CH_4	Th	density/ purity

Table 3.1 Summary of fluid inclusion thermometric data collected based on the three different chemical systems present in inclusions studied. The system H_2O-NaCl is described with and without a solid NaCl phase present because if a solid halite crystal is present in an inclusion at room temperature, the temperature at which the halite dissolves upon heating provides inclusion density (see Figure 4.10). Abbreviations are as follows: Tm, temperature of melting; Th, temperature of homogenization.

CHAPTER 4: RESULTS

4.1 Vein Structure/ Petrography

The microstructural features of the FSBCVs studied include (1) vein parallel wall-rock inclusion layers (WRILs), (2) preferentially oriented, deformed quartz crystals containing subgrains and exhibiting minor undulose extinction, (3) undeformed prismatic tourmaline crystals oriented sub-perpendicular to WRILs and, (4) preferentially oriented FIPs.

4.1.1 Hand Sample Description

FSBCVs are predominantly quartz with minor amounts of sulphide and scheelite. The samples contain abundant WRILs that are parallel or sub-parallel to the vein wall and give the vein a laminated texture (Figure 4.1). These inclusion layers are generally planar but, locally, are stylolitic. They are rarely continuous for more than a few centimetres and are often present as a series of parallel layers that generally form a pyramid shape pointing away from the vein margin (Fig. 4.2). Two domains (discussed below) of quartz have been recognized based on the occurrence of WRILs (Figure 4.2). The veins typically have pinch-and-swell texture on the order of tens of centimetres and range in thickness from about one millimetre to a few centimetres. Figure 4.3 shows the general nature of these veins *in situ*. These veins were observed to be continuous along strike and up and down dip for tens of metres. Many of these veins have slickenlines and/or slickfibres on their margins.

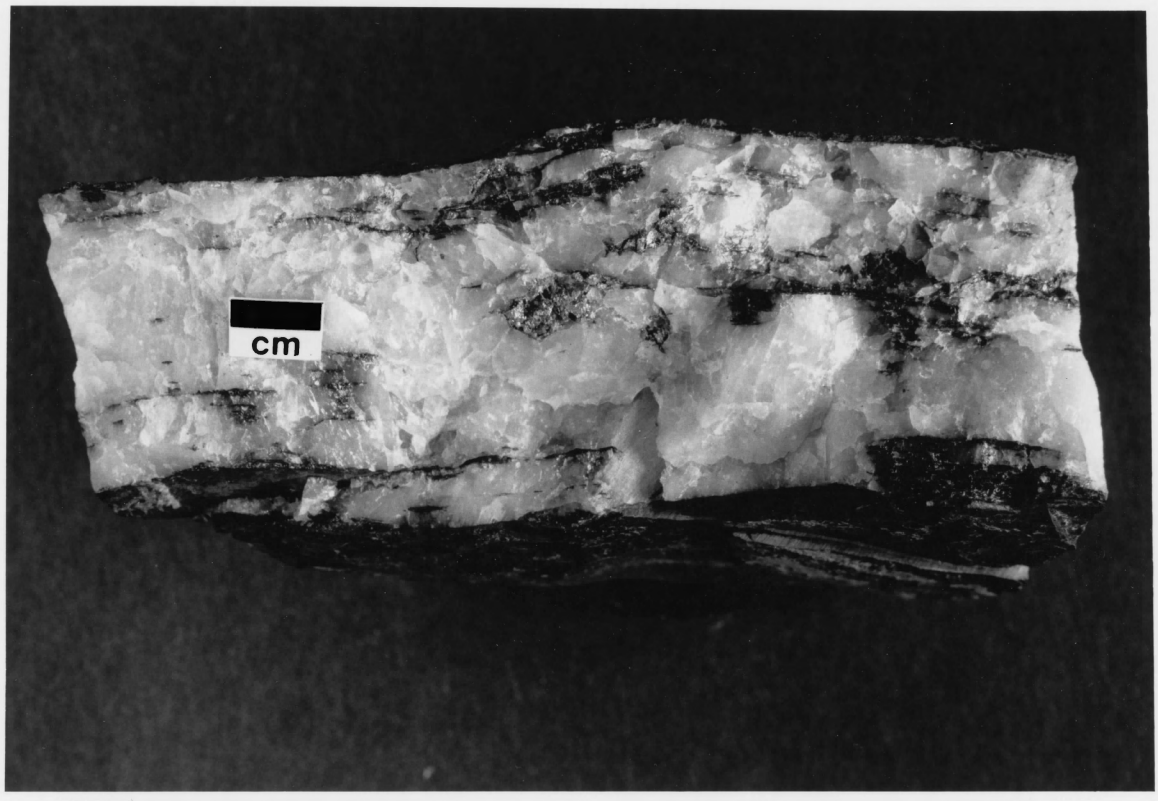

Figure 4.1 Flexural-slip bedding-parallel vein (FSBCV) hand sample O-83.

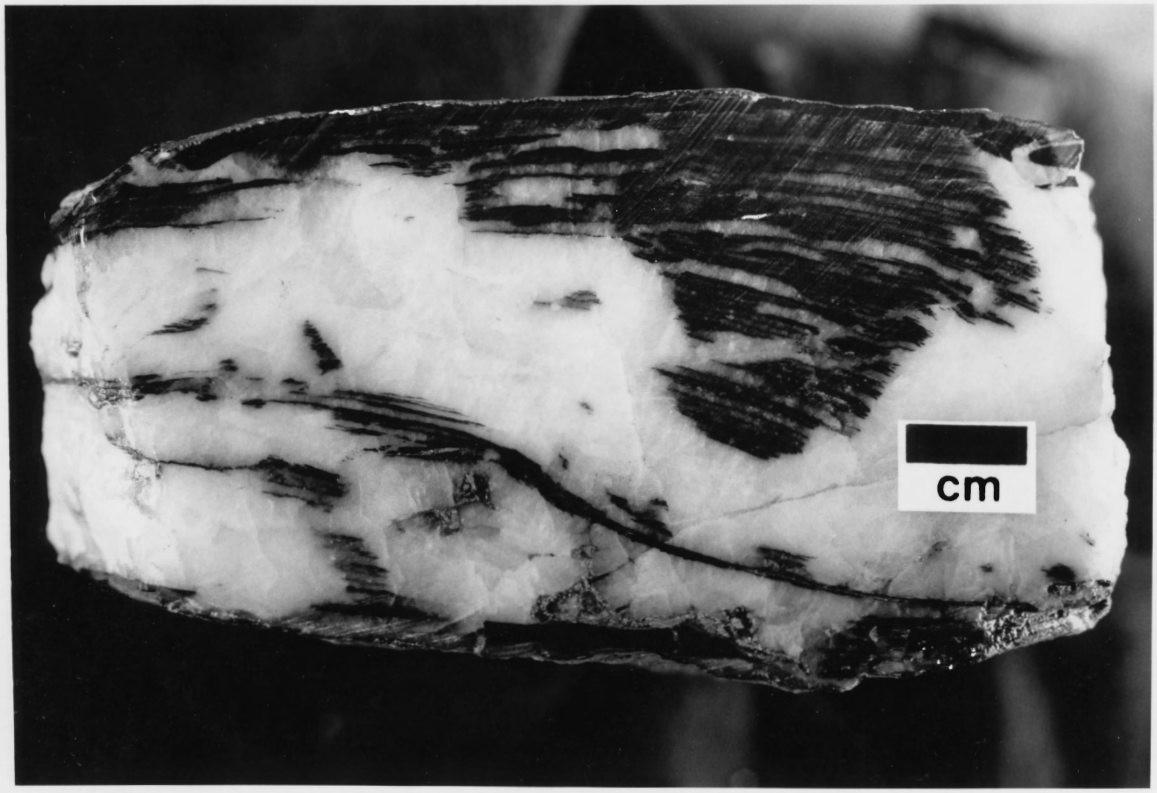

Figure 4.2 Cross-section of sample O-83 with the upper vein margin at the top of the photo. Wall rock inclusion layers (WRILs) are generally more abundant at vein margins. Two domains of quartz, as described in text, are defined by occurrence of WRILs.

Figure 4.3 A typical series of FSBCVs shown viewed down the north limb of the Ovens Anticline. Note abundant veins in slate beds and lack of veins in uncleaved meta-sandstone. Veins pinch and swell and most veins are quite thin as evidenced in this section. Meta-sandstone bed in the centre of the photo is approximately 15 cm thick.

4.1.2 Thin Section Description

4.1.2.1 Wall-rock inclusion layers (WRILs)

Two domains of vein quartz were recognized based on the occurrence of WRILs. Areas that are nearly free of WRILs (Domain I) were distinguished from areas that contain parallel WRILs (Domain II). As well, the two domains show textural differences related to density of fluid inclusions (Fig. 4.4). Domain II quartz contains fewer fluid inclusions and FIPs. As well, the FIPs are generally planar in Domain II quartz whereas FIPs in Domain I quartz are curved. Domain boundaries are not crystal boundaries.

Figure 4.5 shows a series of photomicrographs of WRILs. They are consistently sub-parallel to each other and to the vein margin as described in hand sample. Previous work labelled these structures "inclusion bands" (Henderson *et al.* 1986; Henderson and Henderson, 1986, 1990; Mawer, 1986, 1987), implying a continuous segment of wall-rock that has sharp contacts with adjacent quartz. The term wall-rock inclusion layer (WRIL) has been used here in light of their small-scale lateral irregularity that was observed with a high power zoom microscope which has a greater field of depth than a conventional petrographic microscope. From this perspective, it was noted that thin WRILs (< approximately 15 microns) are not simply continuous bands or sheets of wall-rock material that completely separate layers of adjacent quartz. Instead, they are layers with irregular surfaces and many quartz-filled gaps between wall-rock grains (Figure 4.5a). Thicker WRILs however are solid segments of wall-rock with irregular quartz-wall-rock boundaries.

Adjacent WRILs exhibit complex shapes and relationships with each other. Many

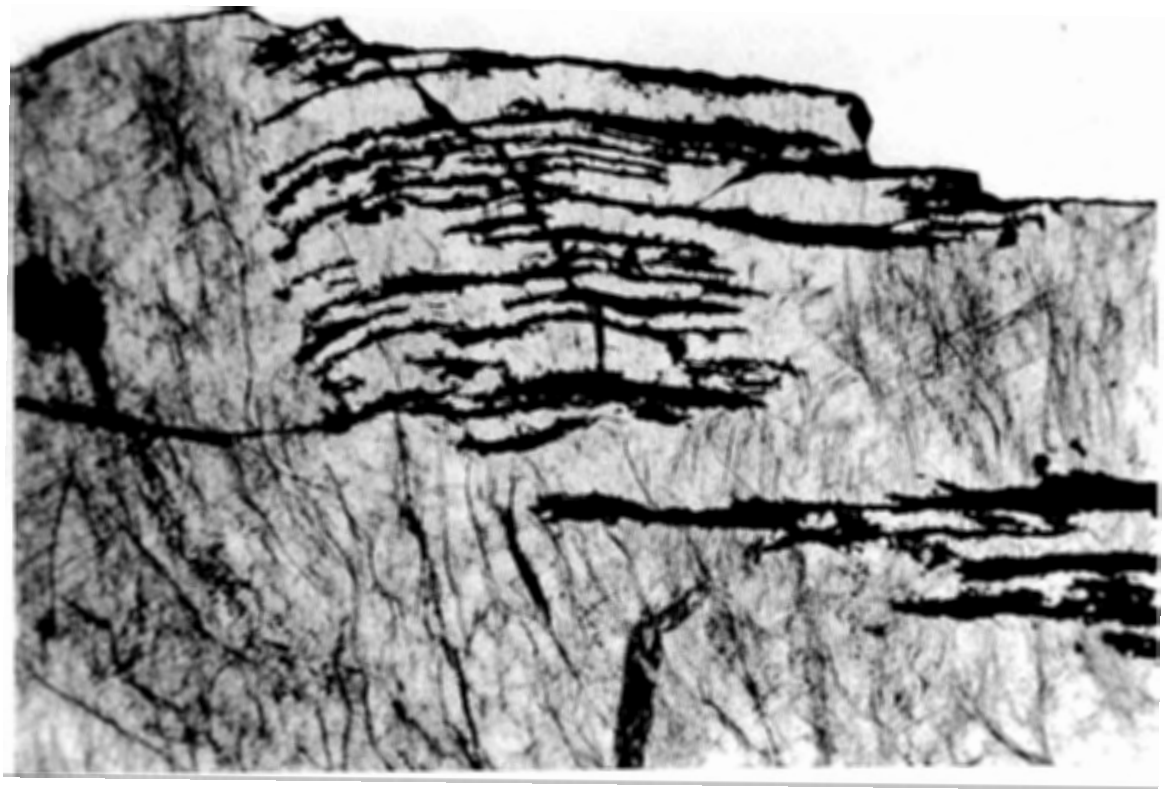

Figure 4.4 Photomicrograph of Domain I and Domain II quartz. Domain I quartz is darker due to a higher density of fluid inclusion planes (faint, linear features) . Domain II quartz is defined by the occurrence of WRILs that separate layers of clearer quartz. Features (fluid inclusion planes, WRILs, laboratory fracture) are exaggerated because the section is a 150 micron thick fluid inclusion section (*cf.* Figure 4.9a) (width of view is 6.5 mm).

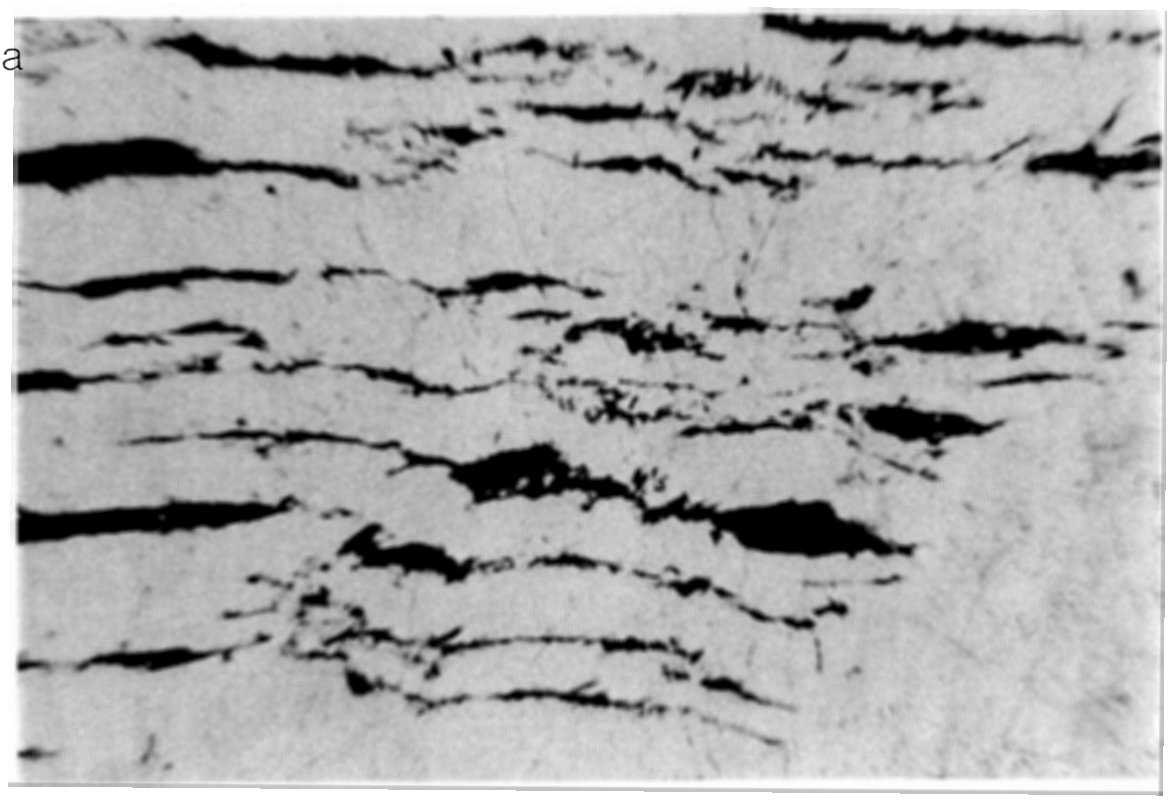

Figure 4.5 Series of photomicrographs from flexural-slip bedding concordant veins (FSBCV) that show evidence of hydraulic fracturing as the mechanism that separated adjacent wall-rock inclusion layers (WRIL). (a) WRILs showing the general irregular wall-rock-quartz contact indicating that these features are not flat bands of wall-rock merely surrounded by quartz, but have chemically or physically been affected by fluids which separated them. Width of photograph is 2.1 mm. (b and c, overleaf) Two examples of corresponding shape and compositional layering that indicates that adjacent WRILs were originally continuous wall rock. Arrows highlight compositional wall rock layers that have been offset. Widths of (b) and (c): 6.5 mm and 1.3 mm respectively.

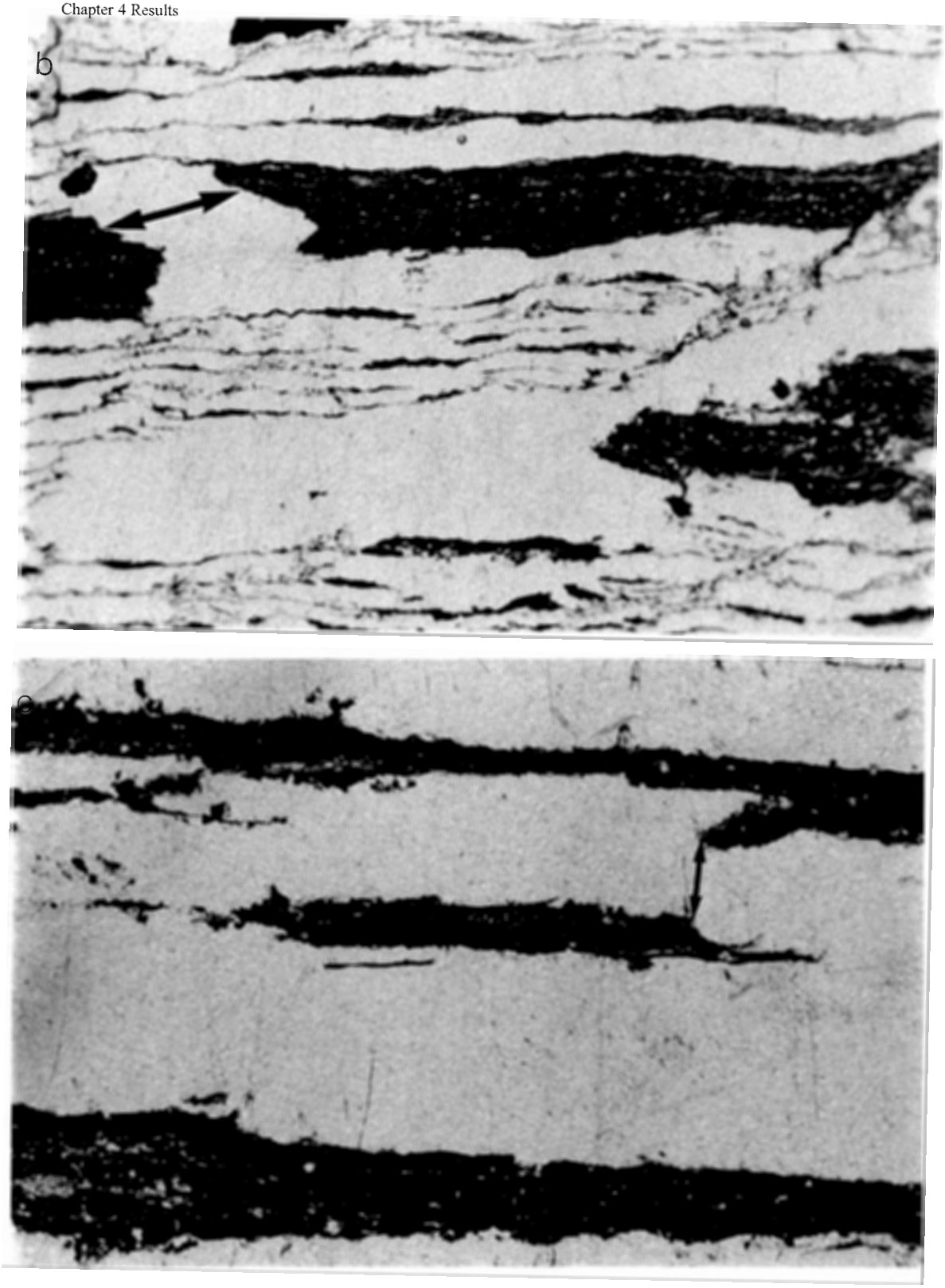

Figure 4.5 (cont'd)

examples of corresponding positive and negative shape pairs are present between adjacent WRILs (Figs. 4.5b and c). As well as corresponding shapes, compositional layers within a WRIL often correspond to layers in a laterally adjacent WRIL (Figs. 4.5b and c, see arrows).

Traverses conducted perpendicular to WRILs across Domain II vein material indicate that an average 17% by thickness is wall-rock while the remainder is quartz. Wall-rock inclusion and quartz layers averaged 35 and 190 microns thick, respectively, but a more meaningful result is the median value because layer thicknesses range through three orders of magnitude. The median thickness of WRILs is 17 microns, whereas the median thickness of quartz layers separating WRILs is 104 microns. Distribution of these data is displayed in the histogram of Figure 4.6.

4.1.2.2 Quartz crystals

C-axis traces (on the thin section surface) recorded for FSBCV quartz crystals show a preferred alignment that has a general correspondence to the crystal elongation direction of larger grains. Figure 4.7 is a line drawing of a complete 150-micron-thick fluid inclusion sections of sample O-60 in two orientations. These record c-axes traces with dashed lines. Note that crystallographic elongation is oblique to the vein wall although this is poorly defined in some areas. The c-axis of two quartz crystals from sample O-83 were also measured with a Universal stage to investigate relationships between FIP and crystallographic orientation. These two points are plotted on the stereo-plots of Figure 4.8a and b.

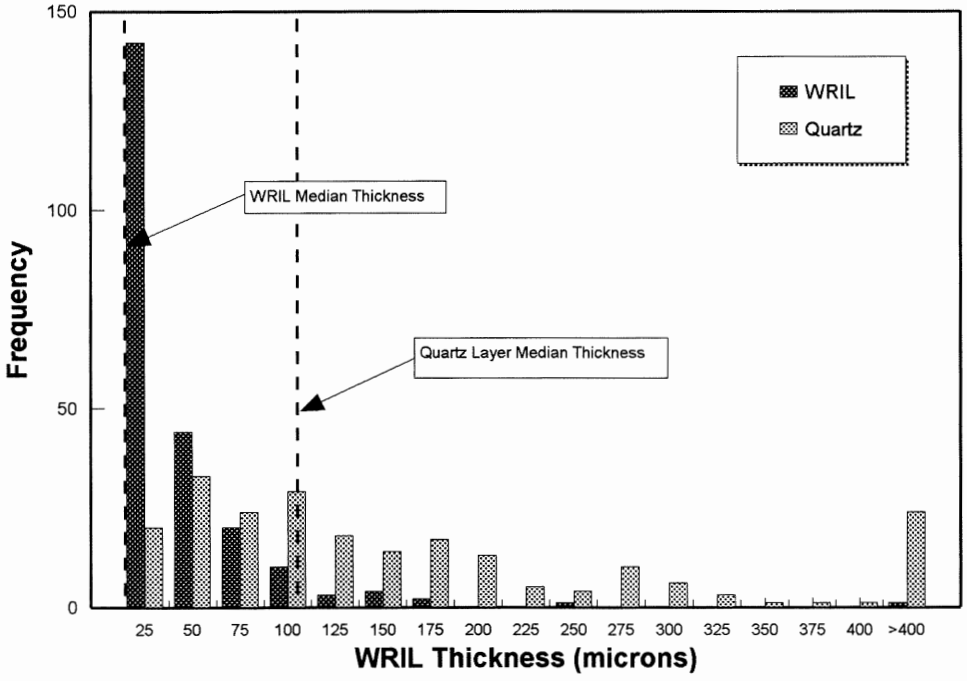

Figure 4.6 Histogram summarizing results of measurements of WRILs and quartz layers in Domain I quartz. Median WRIL thickness is 17 microns while median quartz layer thickness is 104 microns.

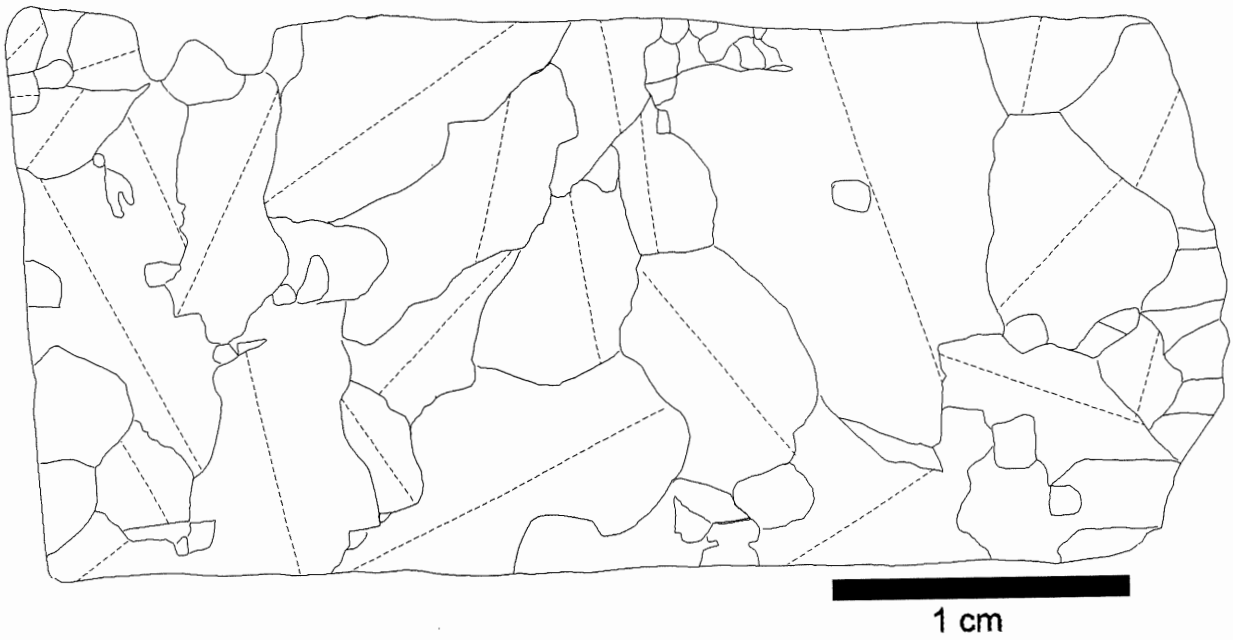

Figure 4.7 Line drawing of quartz crystal boundaries in a FSBCV. Dashed lines are c-axes traces. View is parallel to vein strike (i.e. parallel to the anticlinal hinge).

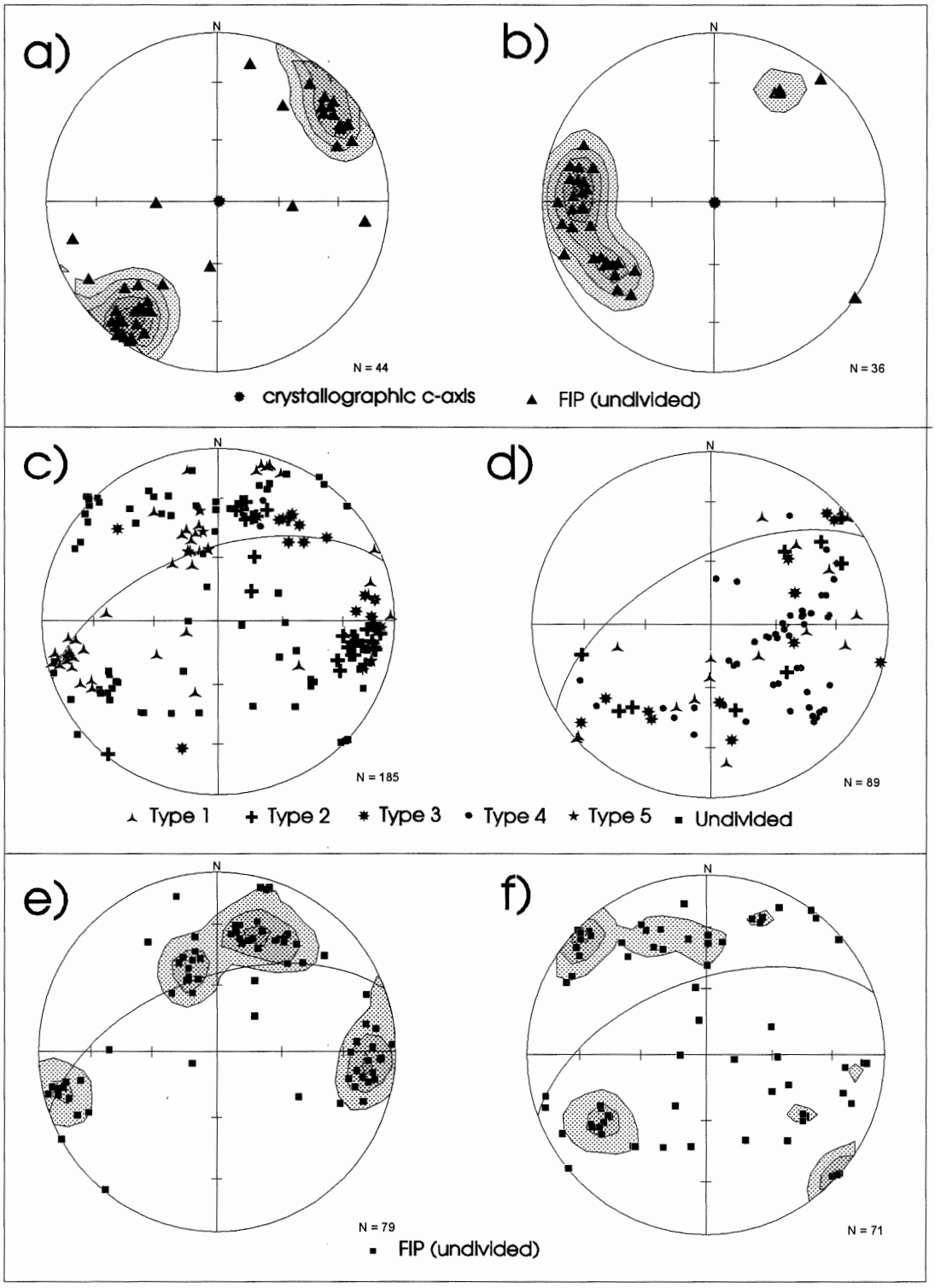

Figure 4.8 Equal area (Schmidt) stereographic projections summarizing FIP orientation measurements. (a-b) FIP orientation compared with quartz crystallographic c-axes. FIP data were recorded from two Domain I crystal grains from sample O-83 (a and b stereo-plots) and then the c-axes of these grains were measured using a Universial stage. All data have been rotated so that the c-axis is at the centre of the stereo-plot. (c-d) Summary of data collected from two thin sections normal to each other (see text) for samples O-83 (c) and O-60, (d). FIPs are divided according to type of fluid inclusion which defined them. Domains I and II quartz. (e-f) Comparison of FIP orientation for Domain I and II quartz from sample O-83: (e) Domain I, (f) Domain II. Data from two thin sections for each Domain. All samples from the north limb of the Ovens Anticline. Great circle represents bedding.

Crystal-plastic deformation of these samples is shown by subgrain development and minor undulose extinction (Figs. 4.9a and b). Crystal grain size is generally large but rare new grains are present. Grain boundaries are sutured (Fig. 4.9a). Deformation lamellae (Knipe 1989) are visible in some crystals as fine, parallel, bright lines that are contained by crystal boundaries.

4.2 Fluid Inclusions

All samples studied from the Ovens contain abundant fluid inclusions. Five distinct morphologic types exist and compositionally these five types fall within three chemical systems. FIPs are preferentially oriented.

4.2.1 Types

The majority of fluid inclusions in samples O-60, O-82 and O-83 was observed to lie in a FIP. No observed inclusions warranted the classification of primary based on the criteria of Roedder (1984). Five types of inclusions were recognized based on size, shape and liquid-vapour ratio at room temperature (Figs. 4.10 and 4.11). As well, imploded fluid inclusions (Sterner and Bodnar 1989) were observed in scheelite from a FSBCV (sample O-25). These structures are shown in Figure 4.11f. Figure 4.12 graphically shows the relative abundance of each type of inclusion for two samples. This information is based on the number of fluid inclusion planes of each type encountered during traverses conducted across thin sections of each sample.

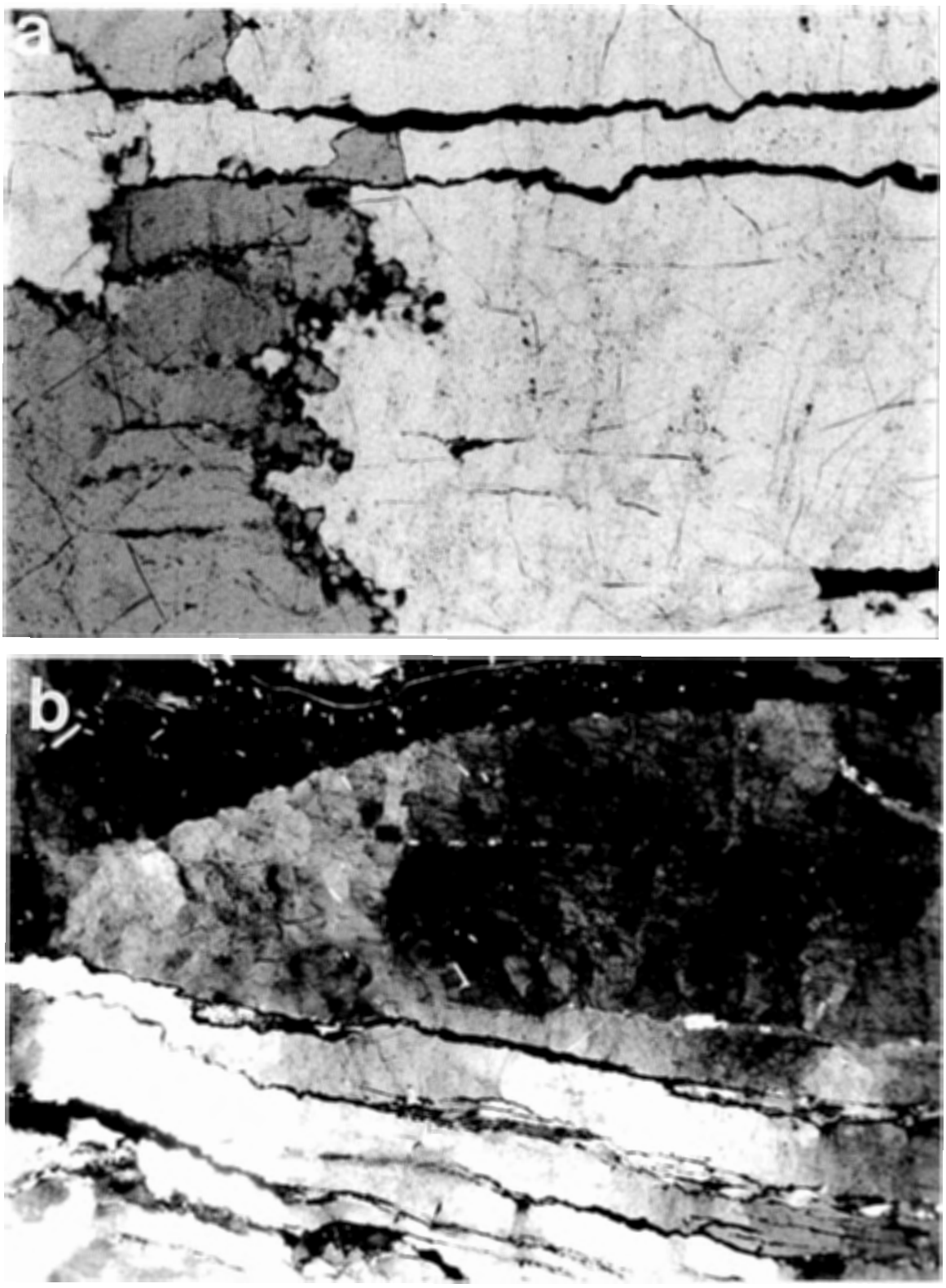

Figure 4.9 Photomicrograph showing (a) subgrains and newgrains and (b) undulose extinction and stylolitic WRILs in a FSBCV.

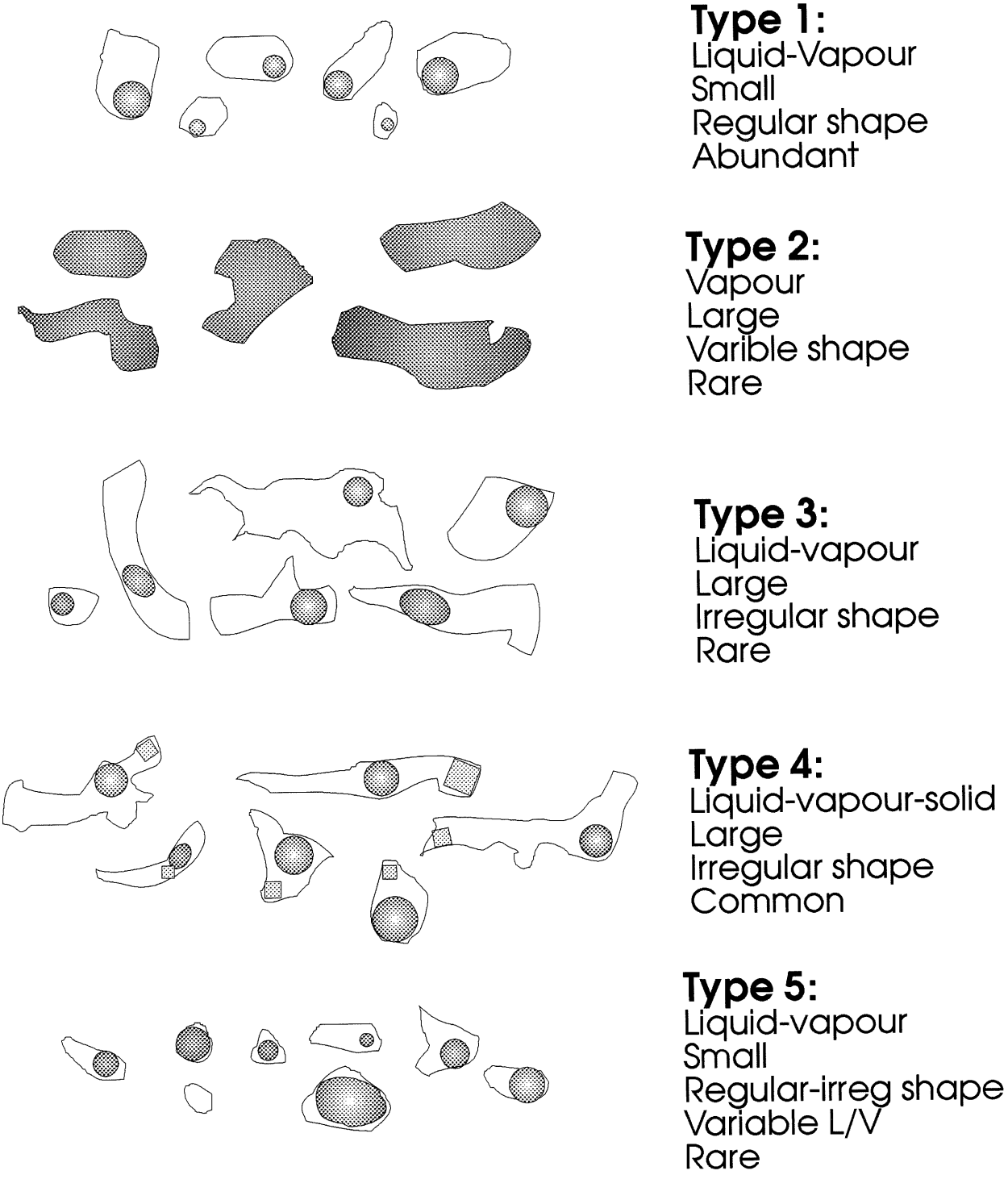

Figure 4.10 Schematic representation of petrograhically distinguished fluid inclusions. All five types are found isolated along planes. Small = 1-3 micron average longest dimension, large = > 6-7 micron average longest dimension.

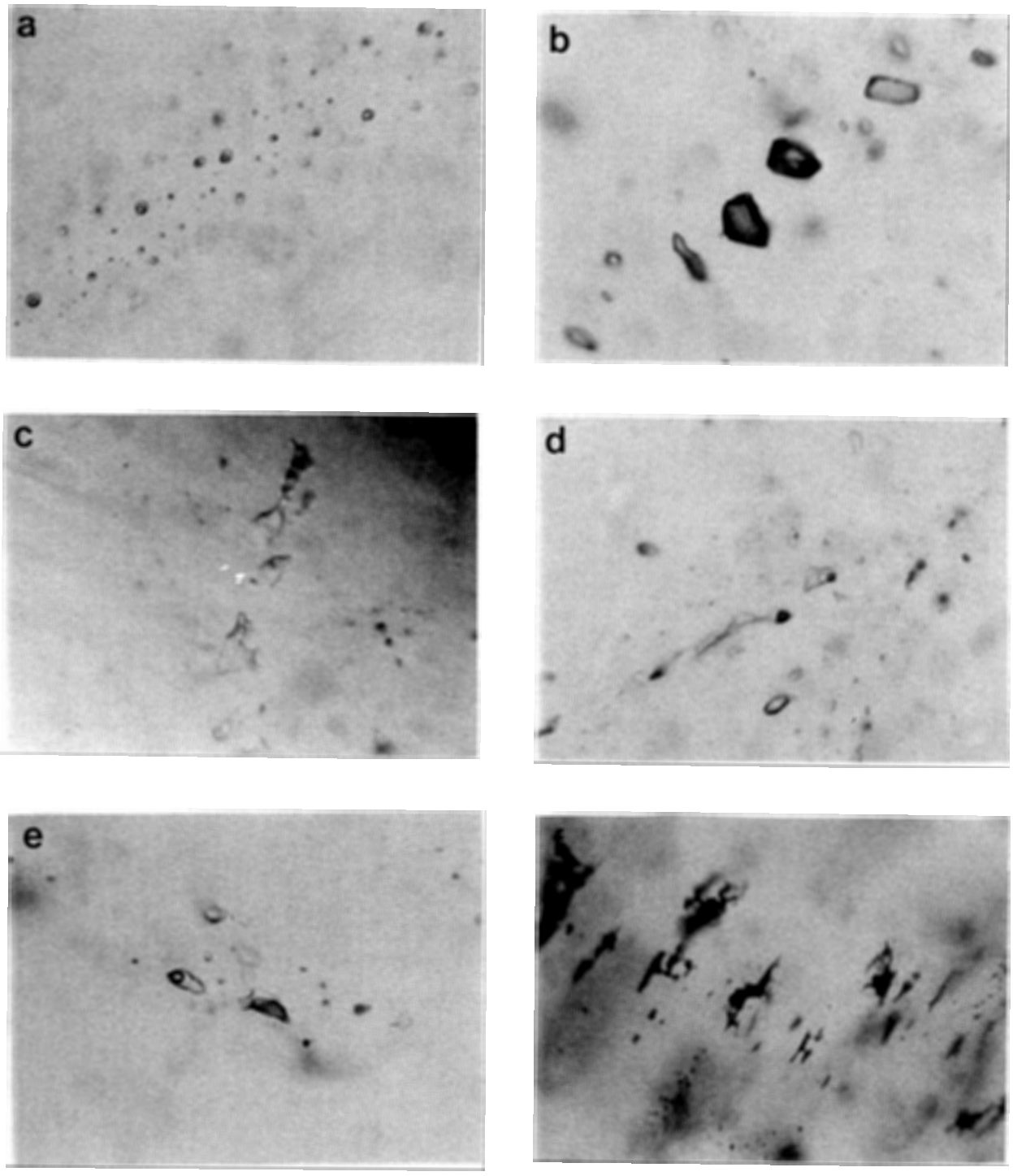

Figure 4.11 Photomicrographs of five petrographically distinguished fluid inclusions. Figures 4.11(a-e) show Types 1-5 respectively. Figure 4.11f is an imploded fluid inclusion from a FSBCV (sample O-25, courtesy R. Horne, Nova Scotia Department of Natural Resources).

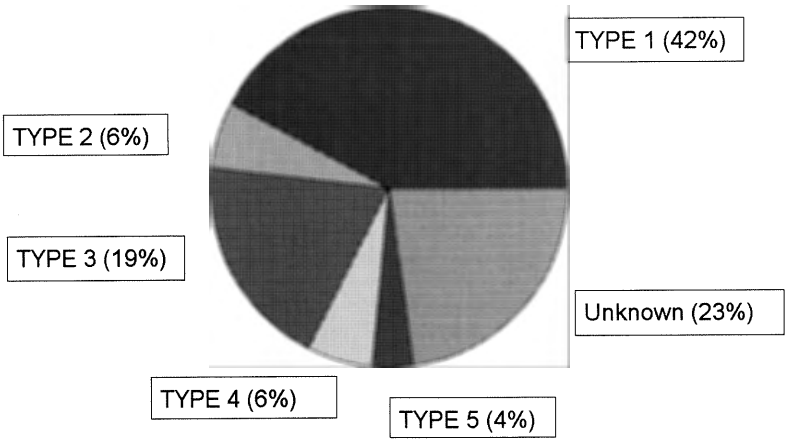

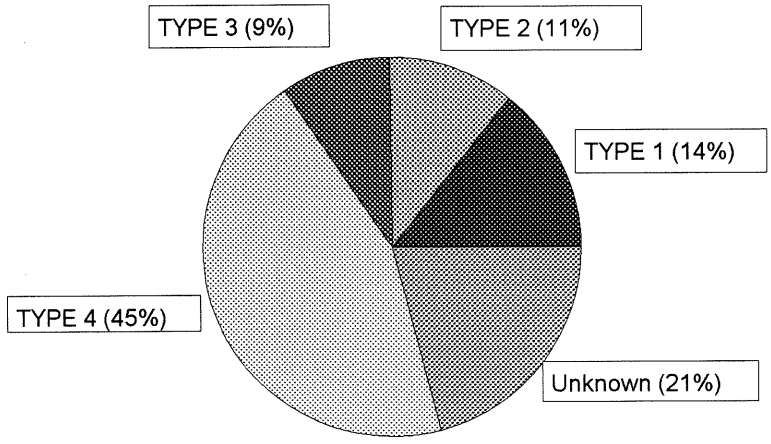

Figure 4.12 Pie graph summary of amount of each type of inclusion in samples (a) O-83, (b) 0-60. Large unknown component due to small inclusion size in many FIPs.

4.2.2 Fluid-Inclusion Plane (FIP) Orientations

Equal-area stereographic projections of FIP orientations are presented in Figure 4.8. These data were collected along traverse lines across fluid inclusion thin sections. Figures 4.8a and b contain poles to FIPs, as well as the c-axes, from single quartz crystals. Figures 4.8c and d contain poles to FIPs plotted according to inclusion type from two samples: O-83 and O-60 respectively. Each plot contains combined data for both Domain I and Domain II quartz. Figures 4.8e and f contain data from sample O-83 for Domain I and Domain II quartz respectively.

4.2.3 Thermometry

Freezing and heating experiments conducted on the five inclusion types indicate that three compositional systems are represented by these inclusions. The behaviour of fluid inclusion phases is schematically summarized in Figure 4.13. Type 1 and Type 3 inclusions belong to the H_2O-NaCl (aqueous) system or the H_2O-NaCl-CO_2 (carbonic) system, Type 2 inclusions contain essentially pure CH_4 or CO_2, Type 4 inclusions are highly saline aqueous and Type 5 inclusions are carbonic.

All observed carbonic inclusions (Fig. 4.10: Type 1, 3 and 5) contain a supercritical CO_2 fluid phase at room temperature. For example, if this phase is observed above its critical density a vapour phase will nucleate upon cooling the inclusion; if below its critical density, a liquid phase will form at the inclusion walls (Roedder 1984). The formation of a liquid CO_2 phase upon cooling was seldom observed, probably due to

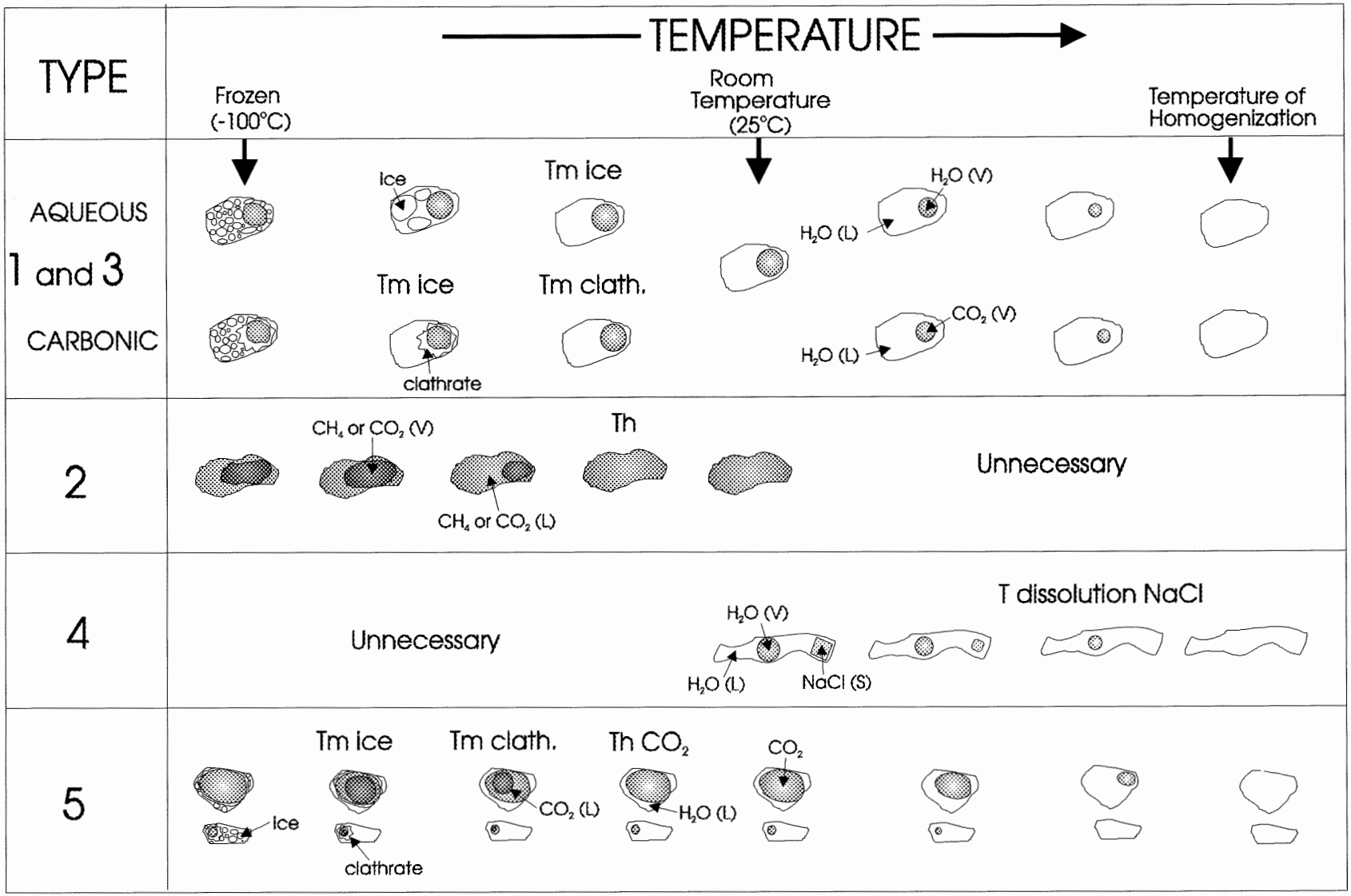

Figure 4.13 Schematic diagram illustrating the behaviour of the five different fluid inclusion types upon heating and cooling. Ice is represented by elipses and clathrate by a jagged outline. Temperatures of melting (Tm) occur on warming from frozen condition. No information is gained from heating Type 2 or freezing Type 4 inclusions. Type 1 and Type 3 inclusions behave the same upon heating and freezing, but are found to be either aqueous or carbonic. Note the temperature scale is independent for each inclusion type.

optical limitations. Nucleation of a vapour CO_2 phase was seldom observed in carbonic Types 1 and 3 inclusions and was always observed in Type 5 inclusions.

In the absence of two visible CO_2 phases, carbonic inclusions can also be distinguished by the formation of CO_2 hydrate (clathrate) at the boundary between H_2O and CO_2 phases upon cooling. This is illustrated in the cooled carbonic Type 1 and 3, and Type 5 inclusions of Figure 4.13, as an exaggerated jagged line surrounding the CO_2 bubble. A sudden, partial collapse of the CO_2 bubble was observed during cooling at temperatures between -30 and -40 °C due to the sudden growth of the clathrate crystals. Type 1 and 3 inclusions were determined to be aqueous if no clathrate or CO_2 vapour formation was observed.

Type 2 inclusions are mixed CO_2-CH_4 inclusions that contain either (a) nearly pure CH_4 or (b) mostly CO_2. These inclusions nucleated a vapour phase upon cooling (see Fig. 4.13) and homogenization temperatures occurred in two groups: -89° to -78° C, and -42° to -25° C. Figure 4.14 is the experimentally determined P-T phase equilibria for the CO_2-CH_4 system. These experimentally derived curves show that the group with lower homogenization temperatures is almost pure CH_4. Certainly, inclusions that homogenized at temperatures below the CH_4, critical point of -82.6° C are pure CH_4, whereas those that homogenized above this temperature contained only slight amounts of CO_2. The group that homogenized at higher temperatures (-42° to -25° C) contains a significant proportion of CH_4 but the data do not permit exact determination of the amount.

Type 4 inclusions are aqueous with at least 26.3 wt. % eq. NaCl. Figure 3.2 is a T-X plot of part of the system H_2O-NaCl. The high salinity portion of this diagram shows

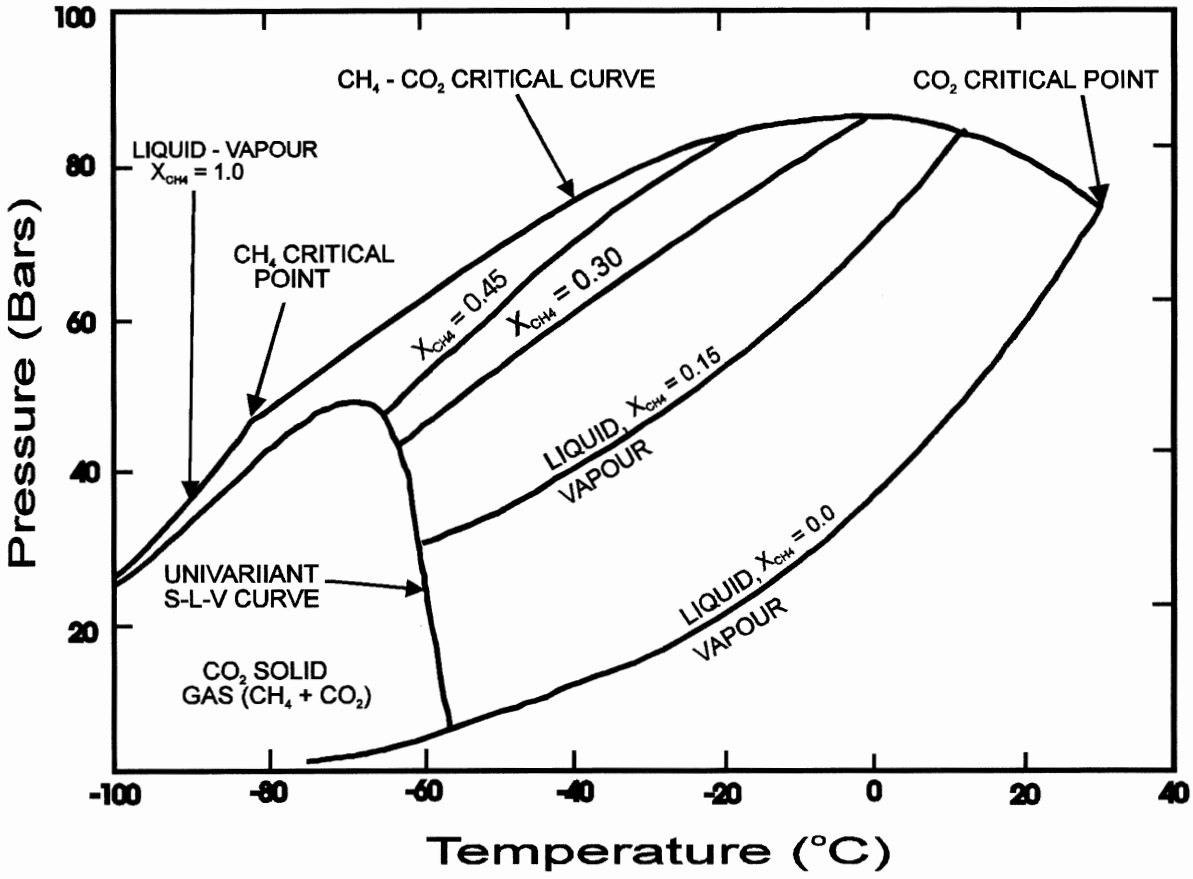

Figure 4.14 Experimental P-T phase equilibria for the system CO_2-CH_4. Inclusions that homogenized below -82.6 °C (CH_4 critical point) follow the liquid-vapour curve and are therefore pure CH_4. Inclusions that homogenized at slightly higher temperatures probably contained slight amounts of CO_2 and, therefore, follow the CO_2-CH_4 critical curve. Inclusions that homogenized in the higher temperature group follow a liquid-vapour curve that connects the univariant solid-liquid-vapour curve and the CO_2-CH_4 critical curve. The exact curve in P-T space cannot be determined because the exact composition is not known. (after Roedder, 1984).

that because Type 4 fluid inclusions contain a solid NaCl phase at room temperature, they fall within the NaCl + Liquid + Vapour phase field and their salinity is constrained to greater than 26.3 wt. % eq. NaCl. The exact salinity is constrained by the dissolution temperature of halite (see curve A, Fig. 3.2).

The composition of aqueous Type 1 and 3 inclusions was determined by the last melting of ice (Tm ice in Fig 3.2). Curve B of Figure 3.2 represents the ice melting point depression with increasing salinity.

Appendix A contains results of freezing and heating experiments on all types of fluid inclusions. Inclusion composition data provided by freezing inclusion Types 1, 2, 3 and 5 and heating of Type 4 inclusions allow determination of inclusion densities (see Chapter 3, Table 3.1). Figure 4.15 shows experimental isochore ranges for the three systems. The use of an independent temperature range (area within vertical dashed rectangle of Figure 4.15) provides an area of P-T space in which each inclusion is inferred to have been trapped. This area was determined from homogenization temperatures of aqueous and carbonic inclusions which represent minimum trapping temperatures (Tt) Figure 4.16 summarizes these data. These results show a range of Tt, however since the data are only a minimum Tt, a range is chosen that accommodates the highest Th measured.

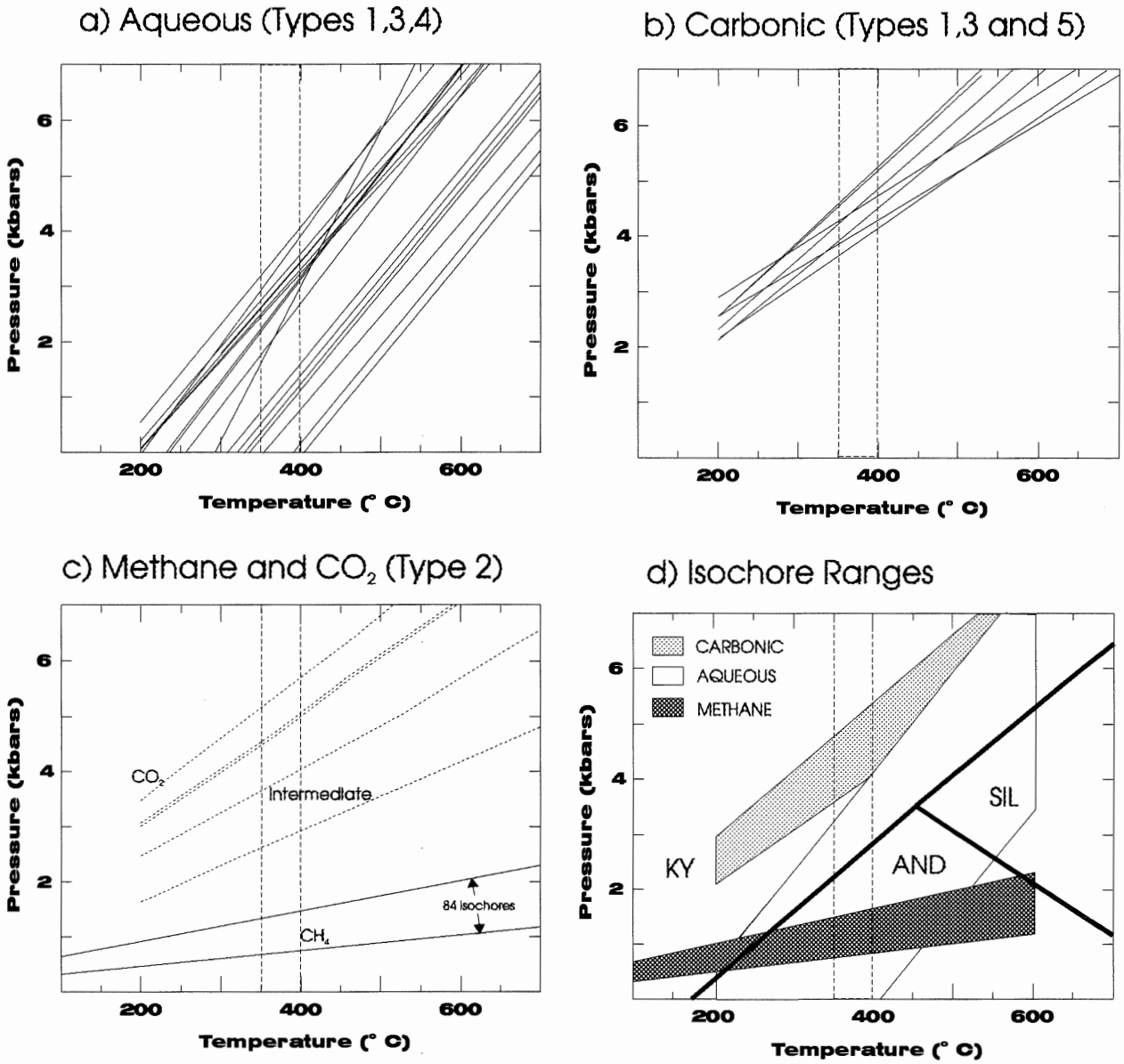

Figure 4.15 Summary of fluid inclusion thermometric results. (a) Results of aqueous inclusions; (b) carbonic inclusions; (c) methane inclusions and 5 isochores from Type 2 inclusions that contain significant proportions of (intermediate), to almost entirely CO_2; and (d) superimposed data from all inclusions.

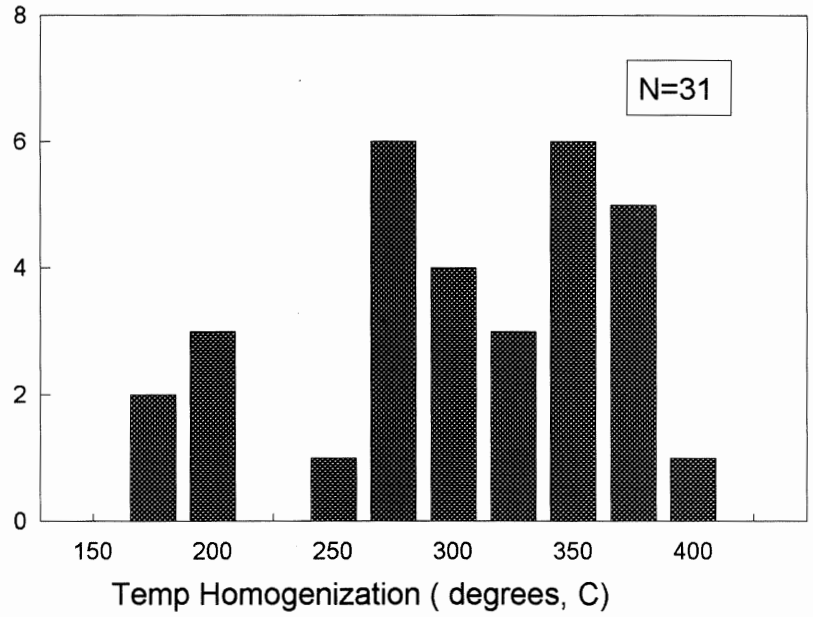

Figure 4.16 Histogram summarizing homogenization data from aqueous inclusions.

CHAPTER 5: DISCUSSION

5.1 Introduction

Much research has been conducted on quartz veins of the Meguma Group and many of the features observed in this study have been reported by previous workers (e.g. Henderson and Henderson, 1987, 1988, 1990; Horne and Culshaw 1994; Mawer, 1986, 1987). Different models exist for the formation of Meguma Group veins: timing and mechanism(s) of formation are the key components of these models.

Pre-folding formation models for Meguma Group veins propose that they formed by hydraulic fracturing (fluid over-pressured) in flat-lying, unfolded sediments (Graves and Zentilli 1982; Henderson and Henderson 1986; Henderson *et al.* 1990). The saddle reef model proposes late syn-tectonic, structurally controlled vein formation in dilatant hinge zones and along bedding planes (leg reefs) (Mawer 1986; Keppie 1976; Faribault 1899; Horne and Culshaw 1994). Vein emplacement related to fluid migration along regional sub-vertical shear zones has also been proposed (Kontak *et al.* 1990).

Based on field relations of quartz veins at the Ovens, Horne and Culshaw (1994) distinguished four vein types based on morphology and the relationships between veins and the fold structure (Figure 2.3). Most previous research did not classify veins according to their relation to the regional structure but has rather described them morphologically. Few workers discussed the possibility that vein formation may have spanned a considerable time period of folding. Work by Horne and Culshaw shows that vein formation spans the timing of fold formation (*cf.* EBCVs and FSBCVs, Chapter 2, Fig.

2.3). This evidence allows for more than one formation model to be responsible for vein formation on the basis that different veins have different times and conditions of emplacement (Horne and Culshaw 1994). Because this thesis focuses only on the FSBCVs, drawing comparisons with other works that may not have constrained vein types must be done with care. This is particularly important with respect to bedding-concordant veins that are often grouped as a single type.

5.2 Mechanisms of Vein Formation

Different mechanisms of quartz vein formation have been proposed to explain micro- and macrostructure of Meguma group veins. Repeated hydraulic fracturing events with later deformation (Mawer 1986), precipitation of vein material from fluid forming "water sills" before folding (Henderson and Henderson 1990), and hydraulic fracturing before folding (Graves and Zentilli 1982; Henderson and Henderson 1986) have been proposed.

Similarities between the Lachlan Fold Belt in central Victoria, Australia and the Meguma Group have long been recognized (e.g. Boyle 1986). The Lachlan Fold Belt is a meta-turbidite, chevron-style fold belt that has historically produced large quantities of gold. Cox *et al.* (1991) provided an overview of many of the goldfields of this area, stressing structural control of veining. These deposits show many of the same features recognized at the Ovens: saddle reefs with accommodation structures in hinge zones, anomalous veining in hinge zones, slickenlines and slickenfibres parallel to dip, and planar, bedding-concordant laminated veins on limbs that formed during flexural slip (Cox

et al. 1991). Antitaxial crack-seal (Ramsay 1980) vein formation (i.e. vein formation consisting of fibrous quartz crystals growing by accretion of vein material at vein margins) in bedding parallel veins from the Lachlan fold belt have been reported (Cox 1987; Jessel *et al.* 1994). Microstructural observations provide the basis for these conclusions. A complex series of 'inclusion surface traces' associated with fibrous quartz crystals are described by Jessel *et al.* (1994) and are interpreted to represent translation and extension paths indicative of movement during flexural-slip vein formation. Cox (1987) concludes that crack-seal veins do not necessarily contain fibrous crystals but can have laminated or irregular crystalline textures. Crystal elongation in the veins studied here is poorly defined and does not represent fibrous crystal growth as described by these authors, although it may be a remnant of a fibrous texture that has been altered by later deformation (Cox 1987).

The crack-seal mechanism of vein formation is defined by Ramsay (1980) as "...an accretionary process involving the formation of a narrow fracture followed by filling of the open space by crystalline material..." As crack-seal events occur, inclusion bands grow in optical continuity with wall rock grains at vein margins (antitaxial vein growth), then become separated and incorporated into the vein by further crack-seal events (Ramsay 1980). The result is narrow inclusion trails composed of many optically continuous mineral grains. This texture was not observed in the veins studied here although inclusions of wall rock are abundant (see WRILs, Fig. 4.5).

WRILs described in Chapter 4 give FSBCVs a laminated appearance and have been described as forming by numerous individual hydraulic fracturing events (Mawer

1986) and therefore meeting the above definition of crack-seal. However, the lack of antitaxial crack-seal textures as described by Ramsay (1980) warrants caution of using this term. Many authors have described the laminated nature of these veins (Mawer 1986; Henderson and Henderson 1987; Henderson *et al.* 1988; Henderson and Henderson 1990). Features observed in this study indicate that adjacent WRILs were originally continuous. As described above, the photomicrographs of Figure 4.5 show adjacent WRILs that have equivalent positive and negative shapes as well as corresponding compositional layering (Figures 4.5b and c). "Rebuilding" of WRILs is not always possible without space problems. Some wall-rock material that became incorporated into vein precipitating fluid was possibly removed either physically by fluid motion, or chemically by fluid-wall rock interaction. Occasional discordant wall-rock segments indicate that some wall-rock may become separated and moved by fluid. Undeformed tourmaline crystals are abundant and associated with WRILs. These provide evidence that WRILs reacted with fluid.

A further argument can be made that the view provided by the thin section may not allow the originally continuous sections of wall-rock to be observed. If the section is cut oblique to the opening direction of the WRILs, one half of the opening pair may be lost due to cutting. Since the median thickness of WRILs is only 17 microns (Fig. 4.6), cutting of the thin section at only a small angle to the opening direction of the WRILs could have a large effect on thin section preservation of corresponding WRILs.

5.3 Fluid Pressure Cycling and Implications of Vein Formation

The results from fluid inclusion study shown in Figure 4.15 constrain the formation pressure of fluid inclusion types as having formed within the given range. Combined with fluid inclusion homogenization temperatures, formation pressures are further constrained to the shaded box of Fig. 4.15 representing a temperature of formation of 350-400°C and pressures from 0.5 to 5.0 kbars. Although this temperature is an estimate, it is fairly well constrained by the Th data which indicate that this temperature range must be accommodated for inclusions since Th data were in this range. Since temperature in such - deposits can not fluctuate very rapidly, it is assumed that all inclusions formed under quite similar temperatures within this range.

Three sources of pressure must be considered important in analyzing these results: lithostatic stress, hydrostatic stress, and fluid overpressure. Given a point of interest at depth in the earth's crust, lithostatic pressure results from a column of rock that applies a downward force on this point and is represented by a lithostatic pressure gradient that varies with depth. If a fracture links the point of interest to the surface watertable, the pressure acting on the point of interest follows a hydrostatic pressure gradient that is equivalent to an overlying column of water. A portion of the calculated pressure of formation of the secondary inclusions studied was due to one, or a combination of hydrostatic and lithostatic pressures since these inclusions were trapped at some depth. The presence of discordant veins at the Ovens Anticline indicates that hydrostatic pressure gradients may have been active if pore fluids may have been connected to the watertable.

Superimposed on Figure 4.15 is the kyanite-sillimanite-andalusite stability field

diagram. Based on metamorphic minerals present, wallrock hosting veins within the Ovens Anticline has not undergone regional metamorphism of grades greater than andalusite grade. The maximum component of pressure that can be attributed to the lithostatic pressure gradient is therefore bounded by the andalusite stability field. Since the data presented here exhibit pressures above this field, it is concluded that the component of the overall pressure that is above the andalusite stability field is due to supralithostatic fluid pressure. If an hydrostatic pressure gradient was active it would decrease the effective overburden pressure and therefore would not affect the conclusion that supralithostatic fluid pressures were present.

Fluid inclusion implosion structures found in coarse scheelite in a FSBCV (Fig. 4.11f) provide further evidence for fluid overpressuring. Imploded fluid inclusions have been experimentally created by formation of inclusions at low pressures, then exposing the same inclusions to high pressure (Sterner and Bodnar 1989). These structures were not observed in quartz, including quartz immediately adjacent to scheelite grains containing implosion structures. This may reflect different physical or mechanical properties of these two minerals.

If the inclusions are secondary and pseudosecondary fluid inclusions it is not possible to state that the experimental pressure results for a given vein represent the pressure of formation of this vein. However, it has been shown that the formation of FSBCVs and associated bedding-discordant veins have an overlapping timing of formation. That is, FSBCVs and bedding-discordant veins are both observed cutting each other (Horne and Culshaw 1994). In the case of a FSBCV cutting an earlier bedding-

discordant vein, the bedding-discordant vein shows offset along the movement horizon that is coincident with the FSBCV. Given this overlapping time relationship and actual separations of up to few metres of bedding-discordant vein along a single movement horizon, it is probable that the fluid trapped in the inclusions studied was responsible for precipitation of other veins as well as healing of microfractures in pre-existing veins.

5.4 Fluid Pressure and Folding

Price and Cosgrove (1990) provide a rigorous discussion of the relationship between flexural-slip fold initiation and the role fluid pressure plays in decreasing effective bodyweight of buckling units. As the ratio of fluid pressure to lithostatic pressure approaches unity, the effective body weight of the buckling unit (e.g. stratigraphic unit) approaches zero. Price and Cosgrove (1990) conclude that without this effect of fluid pressure, the buckling stress required to form a large flexural-slip fold would be greater that the limit of shear failure of most rocks. Such a condition would promote thrusting rather than flexural-slip folding.

Flexural-slip folding occurred late in the folding history of the Ovens Anticline (Horne and Culshaw 1994) but it is not known if flexural-slip is responsible for fold initiation. Outcrop-scale duplex structures (Horne and Culshaw 1994) occur locally on the southern limb of the Ovens Anticline. These are interpreted as early structures because, between duplexes, an interpreted pre-folding bedding-cleavage (approximately 90°) relationship is maintained. That is, between these duplexes no flexural shear has occurred as cleavage has not rotated to an axial-planar orientation. All shortening was therefore

taken up by thrusting that formed these duplexes and is analogous to large-scale flexural slip. Stress required to overcome bodyweight of a folding unit decreases rapidly with increasing dip of the unit relative to the compressive stress field (Price and Cosgrove 1990). The implication of this is that later in the folding history, the stress which must be overcome for flexural-slip folding to occur is reduced.

5.5 FIP Orientations

Results from measurement of FIP orientations indicate that interpretation of these data requires consideration of the following: (a) which type of inclusion populates the FIP; (b) which quartz domain hosts the FIP; (c) crystallographic orientation of the quartz grain which hosts the FIP; (d) FIP orientation with respect to predicted stress conditions on the limb of a flexural-slip fold; (e) comparison with discordant vein orientation and (f) the degree of accuracy attained in measurement of FIPs on a flat stage. Figure 4.8 summarizes the data collected. It is noted that these data are very limited and do not explain FIP orientation with regard to formation conditions or mechanism, but do show that there is a preferred orientation of FIPs.

FIP measurement was incorporated into this study to investigate the possible relationship that FIPs may have with flexural-slip related stress conditions. Initially it was assumed that FIPs represent healed microfractures (Roedder 1984; Smith and Evans 1984) and that orientation of these microfractures would provide paleostress directions since microfractures would open parallel to the least principal stress direction. This technique has been used to determine paleostress conditions from quartz grains in

granitoid rocks (Dula 1981; Lespinasse and Pecher 1986; Laubach 1989; Ren *et al.* 1989).

Recognition that quartz c-axes are preferentially aligned (Fig. 4.7), and preliminary FIP data that are not readily explicable by expected stress conditions, indicated that the assumption that FIPs are healed Coulomb microfractures should be questioned. FIP data will be discussed with regard to two possibilities: (a) FIPs are healed microfractures and their orientation is related to stress conditions, or (b) FIPs are not healed microfractures but their orientation is crystallographically controlled.

Data in Figures 4.8c and d are not easily interpreted as related to stress conditions predicted for flexural-slip folding. However, comparison of Figure 4.8c with orientations of conjugate discordant veins (Figure 5.1) indicates that some FIP data clusters may be oriented the similar to discordant veins and therefore may be related to predicted stress conditions. These data are quite scattered, however, and only some FIP data corresponds to discordant vein oreintation. Data from Figure 4.8d shows no corresponding relationship to discordant vein sets.

3-D orientation of c-axes were measured for two quartz grains using a Universal stage and compared with FIP orientation data from the same grains. Figures 4.8a and b present this data. The star in the centre of these plots represents the c-axis and the remainder of the data are poles to FIPs rotated relative to a vertical c-axis. Comparison of these data with known quartz crystal faces (dipyramids, i.e. crystal terminating faces; Klein and Hurlbut, 1993: pg. 85-87) shows that FIP orientation may correspond to these crystal faces. This may imply that fluid inclusions became trapped during primary crystal growth and that this growth occurred in generally one direction with one crystal face

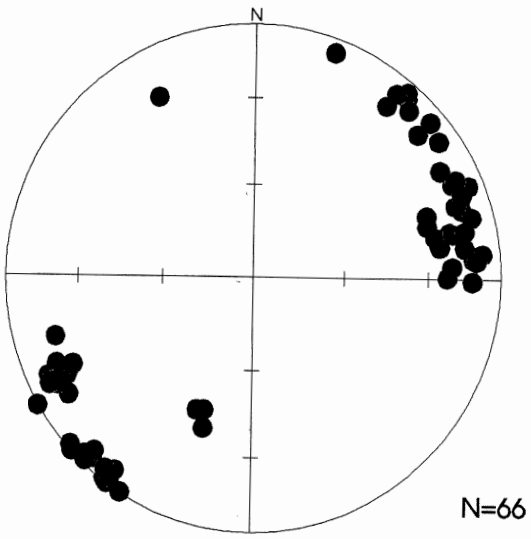

Figure 5.1 Stereographic projection of poles to discordant veins within the Ovens Anticline (data courtesy R. Horne).

dominating. The data of Figures 4.8a and b are however incomplete. Despite these data being recorded from the same sample, the c-axis and FIP data are from different thin sections and the technique used for FIP measurement was not appropriate for measuring planes that were at angles less than about 15° to the thin section (a second section was not measured). As well, this data is from Domain II quartz only.

The only comparison of Domain I and II FIP orientation is between Figures 4.8e and f. These data are combined from two thin sections each (cut parallel and perpendicular to vein dip) for the same sample. Figure 4.8f consists of scattered data from Domain I quartz. These data were from different crystals and the inclusion type is not divided. The lack of correlation between these plots indicates that WRILs may play a role in controlling either the orientation of crystal growth or microfracturing of quartz.

CHAPTER 6: CONCLUSIONS

In this study, microstructural and fluid inclusion analyses were conducted on flexural-slip bedding-parallel veins (FSBCV) from the Ovens Anticline. These data indicate that emplacement of these veins occurred under fluctuating supralithostatic fluid pressure conditions and that vein formation occurred by hydraulic fracturing. These conclusions concur with known flexural-slip folding of the Ovens Anticline.

A range of fluid inclusion isochore lines from different inclusions indicate that fluid pressure was variable during formation of these veins. Results indicate pressures from 0.5 to 5.0 kbars for inclusion entrapment. Given the metamorphic grade of the host rocks, lithostatic pressure can only account for a maximum of 2.8 kbars of this pressure. Any excess pressure is therefore concluded to be a result of fluid pressure. Microstructure of these samples indicate that the veins were opened by hydraulic fracturing. These data are in accordance with late-stage, flexural-slip folding of the Ovens Anticline.

An oriented fluid inclusion plane (FIP) study indicated that FIPs are preferentially oriented. FIP orientation data were appraised (a) with respect to fold-related stress conditions and (b) with respect to quartz crystallography. Findings are inconclusive. Comparison with expected stress conditions indicates that the orientation of these structures was not influenced by regional stress conditions as initially assumed. FIP data indicate that fluid inclusions along FIPs may have become trapped on crystal faces since stereographic projections of data show grouping of FIPs at known quartz crystal terminating faces. Because these data are only from two crystals, a definitive statement to

this effect is not possible, but strongly suggests that FIP orientation is crystallographically controlled.

Recommendations for future work include: (a) further oriented FIP study to compare FIP orientation with crystallography; (b) study to evaluate the preferred orientation of vein crystals given their preferred elongation and crystallographic orientation; and (c) fluid inclusion assessment of saddle reef and bedding discordant veins from the Ovens to investigate any variations from these vein types.

REFERENCES

Boyle, R.W., 1986. Gold deposits in turbidite sequences: Their geology, geochemistry, and history of the theories of their origin. *In* Turbidite-hosted Gold Deposits, *Edited by* J.D. Keppie, R.W. Boyle and S.J. Haynes. Geological Association of Canada, Special Paper 32, pp. 135-148.

Clarke, D.B., Halliday, A.N., and Hamilton, P.J., 1988. Neodymium and strontium isotopic constraints on the origin of the peraluminous granitoids of the South Mountain Batholith, Nova Scotia. Chemical Geology, **73**: 15 - 24.

Collins, P.L.F. 1979. Gas hydrates in CO_2-bearing fluid inclusions and the use of freezing data for estimation of salinity. Economic Geology, **74**: 1435-1444.

Cosgrove, J.W. 1993. The interplay between fluids, folds and thrusts during the deformation of a sedimentary succession. Journal of Structural Geology, **15**: 491-500.

Cox, S.F. 1987. Antitaxial crack-seal vein microstructures and their relationship to displacement paths. Journal of Structural Geology, **9**: 779-787.

Cox, S.F., Wall, V.J., Etheridge, M.A., and Potter, T.F. 1991. Deformational and metamorphic processes in the formation of mesothermal vein-hosted gold deposits-examples from the Lachlan Fold Belt in central Victoria, Australia. Ore Geology Reviews **6**: 391-423.

Cox, S.F. 1995. Deformational Controls on the Genesis of Vein-related Gold Deposits. Conference Abstracts, Gold in Central Victoria, 125th Anniversary Symposium. University of Ballarat, 21 April, 1995.

Cox, S.F., Etheridge, M.A., and Wall, V.J. 1986. The role of fluids in syntectonic mass transport and the localization of metamorphic vein-type ore deposits. Ore Geology Reviews **2**: 65-86.

Douglas, V.G. 1948. Structure of the gold veins of Nova Scotia. *In* Structural Geology of Canadian Ore Deposits. Canadian Institute of Mining and Metallurgy, Jubilee Volume, pp. 919-926.

Dula, W.F. Jr. 1981. Correlation between deformation lamellae, microfractures, macrofractures, and *in situ* stress measurements, White River Uplift, Colorado. Geological Society of America Bulletin, **92**: 37-46.

Ellis, A.J., and Golding, R.M. 1963. The solubility of carbon dioxide above 100°C in water and in sodium chloride solutions. American Journal of Science, 261: 47-60.

Faribault, E.R. 1899. On the gold measures of Nova Scotia and deep mining. Canadian Mining Review, **18:** 78-82.

Gehrig, M., Lentz, H., and Franck, E.U., 1979. Thermodynamic properties of water-carbon dioxide-sodium chloride mixtures at high temperatures and pressures. *In* International Conference on High Pressure Science and Technology: Volume I, Physical Properties and Materials Synthesis. *Edited by* K.D. Timmerhaus and M.S. Barber. Plenum Press, New York, New York.

Goldstein, R.H., and Reynolds, T.J. 1994. Systematics of Fluid Inclusions in Diagenetic Minerals. Society for Sedimentary Geology short course 31.

Graves, M.C. and Zentilli, M. 1982. A review of the geology of gold in Nova Scotia. *In* Geology of Canadian Gold Deposits. *Edited by* R.W. Hodder and W. Petruk. Canadian Institute of Mining and Metallurgy, Special Volume 24, pp. 233-242.

Haynes, S.J. 1986. Geology and geochemistry of turbitdite-hosted gold deposits, greenschist facies, eastern Nova Scotia. *In* Turbidite-hosted Gold Deposits, *Edited by* J.D. Keppie, R.W. Boyle and S.J. Haynes. Geological Association of Canada, Special Paper 32, pp. 161-177.

Henderson, M.N., and Henderson, J.R. 1986. Constraints on the Origin of Gold in the Meguma Zone, Ecum Secum area, Nova Scotia. Maritime Sediments and Atlantic Geology, **22**: 1-13.

Henderson, J.R., and Henderson, M.N. 1987. Meguma gold deposits; nested saddle reefs or early hydraulic extension fractures? *In* Nova Scotia Department of Mines and Energy Report 87-5, pp. 221-223.

Henderson, J.R., Wright, T.O., and Henderson, M.N. 1986. A history of cleavage and folding: an example from the Goldenville Formation, Nova Scotia. Geological Society of America Bulletin, **97**: 1354-1366.

Henderson, J.R., Wright, T.O., and Henderson, M.N. 1988. Mechanics of formation of gold-bearing quartz veins, Nova Scotia. *In* Nova Scotia Department of Mines and Energy Report 88-3, pp. 221-223.

Henderson, J.R., and Henderson, M.N. 1990. Water-sill hypothesis for the origin of certain veins in the Meguma Group, Nova Scotia, Canada. Geology, **18**: 654-657.

Horne, R.J. 1993. Central Meguma Mapping Project: flexural slip in the Halifax Formation. *In* Program and Summaries, Seventeenth Annual Review of Activies. *Editied by* D.R. MacDonald, Nova Scotia Department of Natural Resources, Mines and Energy Branches Report 93-2, p. 3.

Horne, R.J., and Culshaw, N. 1994. Preliminary evaluation of flexural slip as a folding mechanism and its significance in localizing auriferous veins in the Meguma Group, Nova Scotia. *In* Mines and Energy Branch, Report of Activities 1993; Nova Scotia Department of Natural Resources, Mines and Energy Branch Report 94-1, pp. 147-160.

Hubbert, M.K. and Rubey, W.W., 1959. Role of fluid pressure in the mechanics of overthrust faulting. Geological Society of America Bulletin, **70:** 115-205.

Jessell, M.W., Willman, C. E., and Gray, D.R. 1994. Bedding parallel veins and their relationship to folding. Journal of Structural Geology, **16**: 753-767.

Keppie, J.D. 1976. Structural model for the saddle reef and associated veins in the Meguma Group, Nova Scotia. Nova Scotia Department of Mines Paper 76-1, pp. 1-34.

Keppie, J.D., and Dallmeyer, R.D., 1987. Dating transcurrent terrane accretion: an example from the Meguma and Avalon composite terranes in the northern Appalachian. Tectonics, **6**: 831-847.

Klein, C. and Hurlbut, C.S., 1993. Manual of Mineralogy, 21st edition. John Wiley & Sons, Inc.

Knipe, R.J. 1989. Deformation mechanisms-recognition from natural tectonites. Journal of Structural Geology, **11**: 127-146.

Kontak, D.J., Smith, P.K., Kerrich, R., and Williams, P.F. 1990. Integrated model for Meguma Group lode gold deposits, Nova Scotia, Canada. Geology, **18**: 238-242.

Laubach, S.E. 1989. Paleostress directions from the preferred orinetation of closed microfractures (fluid-inclusion planes) in sandstone, East Texas basin, U.S.A. Journal of Structural Geology, **11**: 603-611.

Lespinasse, M., and Pecher, A. 1986. Microfracturing and regional stress field: a study of the preferred orientations of fluid-inclusion planes in a granite from the Massif Central, France. Journal of Structural Geology, **8**: 169-180.

Mawer, C. K. 1986. The bedding-concordant gold-quartz veins of the Muguma Group, Nova Scotia. *In* Turbidite-hosted Gold Deposits, *Edited by* J.D. Keppie, R.W. Boyle and S.J. Haynes. Geological Association of Canada, Special Paper 32, pp. 135-148.

Mawer, C.K. 1987. Mechanics of formation of gold-bearing quartz veins, Nova Scotia Canada. Tectonophysics, **135**: 99-119.

McBride, D.E. 1978. Geology of the Ecum Secum area, Halifax and Guysborough Counties, Nova Scotia. Nova Scotia Department of Mines and Energy Paper 78-1, pp. 1-12.

Muecke, G.K., Elias, P., and Reynolds,P.H., 1988. Hercynian/Alleghanian overprinting of an Acadian terrane: $^{40}Ar/^{39}Ar$ studies in the Meguma Zone, Nova Scotia, Canada, Chemical Geology (Isotope Geoscience), **73**: 153-167.

Newhouse, W.H. 1936. A zonal gold mineralization on Nova Scotia. Economic Geology, **31**: 805-831.

O'Brien, B.H., 1988. A study of the Muguma Terrane in Lunenburg County, Nova Scotia. Geological Survey of Canada, Open File 1823.

Price, N.J. and Cosgrove, J.W. 1990. Analysis of Geological Structures. Cambridge University Press. Cambridge, Great Britain.

Ramsay, J.G. 1974. The Developement of Chevron Folds. Geological Society of America Bulletin, **85**: 1741-1754.

Ramsay, J.G. 1980. The crack-seal mechanism of rock deformation. Nature, **284**: 135-139.

Ren, X., Kowallis, B.J., and Best, M.G. 1989. Paleostress history of the Basin and Range province in western Utah and eastern Nevada from healed microfracture orintations in granites. Geology, **17**: 487-490.

Roedder, E. 1984. Fluid Inclusions. *In* Reviews in Mineralogy. *Edited by* P.H. Ribbe. Bookcrafters, Chelsea, Michigan.

Schenk, P.E., 1991. Events and sea-level changes on Gondwana's margin: The Meguma Zone (Cambrian to Devonian) of Nova Scotia, Canada. Geological Society of America, Bulletin, **103**: 512-521.

Selverstone, J., Axen, G.J., and Bartley, J.M. 1995. Fluid Inclusion constraints on the kinematics of footwall uplift beneath the Brenner Line normal fault, eastern Alps. Tectonics, **14**: 264-278.

Smith, D.L., and Evans, B. 1984. Diffusional Crack Healing in Quartz. Journal of Geophysical Research, **89**: 4125-4135.

Sterner, S.M. and Bodnar, R.J. 1989. Synthetic fluid inclusions-VII. Re-equilibration of fluid inclusions in quartz during laboratory-simulated metamorphic burial and uplift. Journal of Metamorphic Geology, **7**: 243-260.

Tanner, P.W.G. 1989. The flexural-slip mechanism. Journal of Structural Geology, **11**: 635 - 655.

APPENDIX A

Tabulated fluid inclusion thermometric results. Tm = temperature of melting, Th = temperature of homogenization, Td = temperature of dissolution. Numbers separated by a (/) indicate the maximum and minimum values measured for the given fluid inclusion population and the number in brackets is the number of inclusions measured.

Sample	section	chip	location	type	isochore	Tm CO_2	Tm ice	Tm clath	Th CO_2	Th CH_4	Th	Td NaCl
O-60	a	1	1	2		-	-	-	-48/-27 (4)	-	-	-
	a	1	1	1		-	-10/-2.8 (2)	-	3.4/7.0 (5)	-	314/385 (6)	-
	a	1	1	3		-56/-59 (5)	-	-	8.5/27 (5)	-	-	-
	a	1	1	5		-83/-59 (5)	-8.0/-4.5 (2)	5.8/8.5 (4)	8.0/18.0 (4)	-	285	-
	a	1	1	5		-	-	-	8.1 (V)	-	350 (V)	-
	a	4	1	4		-	-	-	-	-	193/285 (5)	235/268 (4)
	a	5	1	3		-	-	-	12.0	-	-	-
	a	5	2	2		-61.6/-60.0 (5)	-	-	-25.0/-2.2 (2)	-	-	-
	a	5	4	3		-59.5/-59.0 (2)	-24.0/-19.0 (2)	-2.5/-1.6 (2)	4.0/3.4 (2)	-	-	-

O-83	a	1	1	2		-	-	-	-	-83.0/-79.9 (17)	-	-
	a	1	4	2		-	-	-	-	-82.0/-79.0 (14)	-	-
	a	3	2	1		-	-6.3/-2.0 (7)	6.1/10.5 (7)	-	-	-	-
	a	3	2	1		-	-	-	-	-	240/347 (6)	-
	a	3	-	1		-	-	-	-	-	264/392 (6)	-
	a	3	2	3		-	-	-	-	-	275/340 (2)	-
	a	3	2	3		-	-	-	-	-	380 (V)	-
	a	3	2	3		-	-	-	-	-	464 (V)	-
	a	3	2	3		-	-	-	-	-	420 (V)	-
	b	1	2	2		-	-	-	-	-88/-79 (22)	-	-
	b	2	1	2		-	-	-	-	-85/-84 (7)	-	-
	b	2	1	2		-	-	-	-	-89/-87 (6)	-	-
	b	2	1	3		-	-16.2/-10.8 (5)	-	-	-	-	-
	b	1	-	1		-	-7.9/-8.0 (2)	2.5/8.0 (2)	-	-	-	-
	b	1	-	5		-66.0	-	-	-23/-4.0 (3)	-	-	-
	b	1	2	2		-	-	-	-	-81/-79 (7)	-	-
	b	1	2	1		-	-16.0/-7.2 (5)	-	-	-	-	168/200 (6)
	b	1	2	2		-	-	-	-	-83/-81 (11)	-	-
	b	3	3	1		-	-7.4	3.1/7.0 (4)	-	-	-	-
	b	3	4	3		-	-10.0/-4.9 (11)	-	-	-	-	-
	a	6	2	4		-	-	-	-	-	218/232 (3)	190/200 (3)